

Lichen dating of earthquake-generated regional rockfall events, Southern Alps, New Zealand

William B. Bull* *Geosciences Department, University of Arizona, Tucson, Arizona 58721*

Mark T. Brandon† *Department of Geology and Geophysics, Yale University, New Haven, Connecticut 06520-8109*

ABSTRACT

Synchronous regional rockfall events triggered by large earthquakes in the Southern Alps of New Zealand were used to evaluate and improve the lichenometry method for surface-exposure dating. Digital calipers were used to measure the maximum diameter of the largest lichen on many rockfall blocks, using a fixed-area largest-lichen (FALL) sampling strategy. Regional significance of FALL peaks can be tested by confirming the occurrence of a coeval peak at multiple sites, and by showing an increase in peak size toward the earthquake epicenter. Significance of FALL peaks at a local site can be described in terms of peak size relative to a uniform density of FALL sizes.

Measurements of 34 000 FALL sizes on fully exposed rockfall blocks and outcrop joint faces at 90 sites allow precise dating of geomorphic events of the past 300 to 500 yr. Uncertainties at the 95% confidence interval can be reduced to a level better than ± 10 yr for ages within the calibrated time range represented by the lichen growth equation. Recognition of prehistorical regional rockfall events in 1833, 1836, and 1840 demonstrates the excellent resolution of this dating method. Precise dates result from exceptionally low measurement errors of lichen sizes relative to their growth rate, tightly clustered FALL sizes for earthquake-induced rockfall events, and substrate exposure times for calibration sites that are known to the year or day.

FALL peaks for synchronous rockfall events are the same for 20 sites with diverse climate, altitude, and substrate lithology. A regionally consistent lichen growth rate allows use of a single growth-rate equation for most

species of *Rhizocarpon* subgenus *Rhizocarpon* on the South Island of New Zealand. A nonlinear growth equation suggests that the first colonization, on average, occurs in the 5th yr after formation of new rock surfaces (~ 0.5 m² unit areas) and is followed by rapid, exponentially declining growth for about 20 yr (great-growth phase) that is largely completed by the 24th yr. Then, linear growth persists at about 15 mm per century (uniform-growth phase).

INTRODUCTION

Lichens can be used to estimate the ages of surfaces of young rocky deposits or the times of recent exposure of outcrops. Lichen sizes record both the initial time of exposure of the rock substrate upon which they grow, and subsequent disturbances to surficial boulders or joint blocks that expose fresh substrates for colonization by younger lichens. The ability to record postformation disturbances also applies to other surface-exposure dating methods, such as weathering rinds and cosmogenic isotopes. Lichenometry directly dates times of specific events, such as earthquakes, by determining the time of earthquake-generated landslides. In contrast, radiocarbon stratigraphic dating estimates the time that organic matter grew. Deposition of organic matter in fluvial, colluvial, or swamp deposits at paleoseismic sites is not directly tied to specific earthquake events, because datable organic matter is created before or after seismic disruption of the stratigraphic section.

Lichenometry dates geomorphic events, and like radiocarbon dating of stratigraphic events, it is in its fifth decade of development. However, lichenometry continues to be hindered by a paucity of widely accepted measurement and analytical procedures (Worsely, 1981), which restricts comparison of results by different workers. In part, the lack of a standard approach has resulted from diverse study areas, each of which

had a different purpose, sampling strategy, and assumptions. Locke et al. (1979) attribute the lack of a universal method to the founder of lichenometry, Beschel (1950, 1957, 1959, 1961, 1963), who emphasized only general guidelines instead of a preferred method. Most workers continue to estimate ages for geomorphic events, such as floods, glacier advances, and landslides, based on the single largest lichen or mean of five largest lichens for the entire deposit. Examples include worthy papers by Matthews (1974), Locke et al. (1979), Birkeland (1981), Porter (1981), Rapp (1981), and Innes (1984, 1985a).

Some recent studies have departed from the conventional approach by sampling populations of largest lichens on many blocks deposited by rockfalls, snow avalanches, glaciers, and debris flows (Bull, 1991a, 1994; Matthews and McCarroll, 1994; McCarroll, 1993, 1994; Luckman and Fiske, 1995). Bull concentrated on dating of earthquake-generated (coseismic) rockfall events in California and New Zealand (Bull et al., 1994; Bull, 1996a, 1996b). His new field and analytical procedures for lichenometry were developed in a variety of geomorphic settings, and have been used to study slush avalanches in northern Sweden (Bull et al., 1995), which has virtually no earthquakes. This paper expands on the lessons learned from Bull's diverse studies to describe a new approach to lichenometry.

We seek to advance lichenometry by emphasizing the benefits of large sample sizes. Digital calipers were used to measure the maximum diameter of the largest lichen on many rockfall blocks in the Southern Alps, where outcrops and hillslopes are disrupted by large earthquakes. About 34 000 lichen-size measurements were made at 90 sites in the South Island of New Zealand (Fig. 1). Measurements were made from 1989 to 1997 and, where necessary, are normalized to 1992 as a reference year. We use the synchronous nature of rockfalls throughout much of our 40 000 km² study region to provide

*e-mail: william.bull@geo.arizona.edu

†mark.brandon@yale.edu

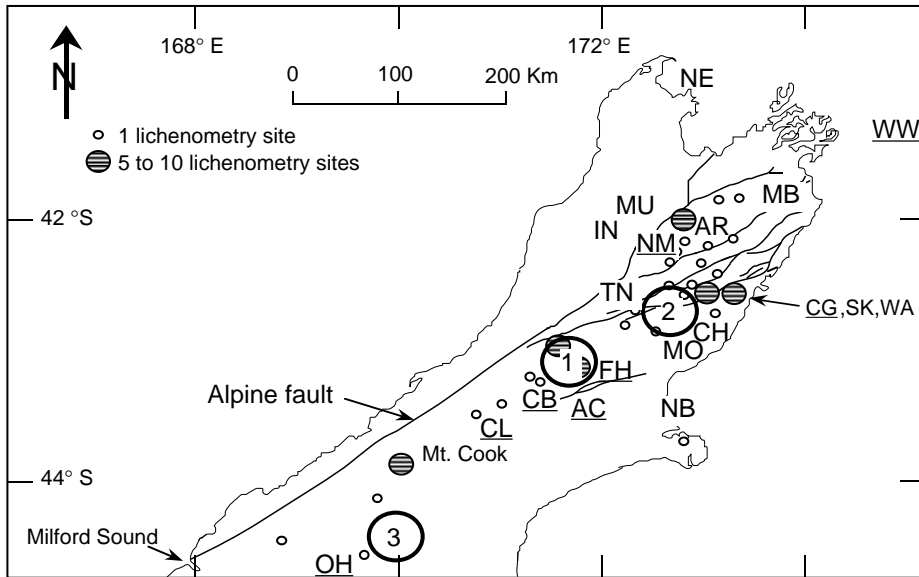


Figure 1. Map of the South Island of New Zealand showing the Alpine fault system and locations of lichenometry sites and historical earthquakes (Table 2). Faults are shown by black lines (Officers of the New Zealand Geological Survey, 1983; Van Dissen and Yeats, 1991). Approximate locations of earthquake epicenters are: AR—Acheron River; CH—Cheviot; IN—Inangahua; MA—Marlborough; MO—Motunau; MU—Murchison; NB—New Brighton; NE—Nelson; SK—Seaward Kaikoura; TN—Tennyson, and WA—Waiiau. The 1855 West Wairarapa earthquake, WW, occurred in the southern part of the North Island. Locations of lichenometry sites are underscored: AC—Acheron rock avalanche; CB—Craigieburn rock avalanche; CG—Cattle Gully; CL—Clyde rock avalanche; NM—No Man's Creek; and OH—Ohaui. Circled 1 indicates the general locations of the Arthur's Pass, Lake Coleridge, and Bealey earthquakes, Falling Mountain rock avalanche, and the Otira Valley, Rough Creek, and Zig Zag sites. Circled 2 includes the North Canterbury and Hossack earthquakes, Raupo Swamp, and the Hope River Bridge landslide. Circled 3 includes the Mueller and Tasman glaciers, and the Celmisia and Idyllic sites.

new insights about factors influencing the precision, accuracy, and resolution of lichenometry as a surface-exposure dating method. Synchronous rockfall events at sites with different altitudes, substrate lithologies, and climatic settings allowed us to determine whether or not calibration of lichen growth rates based on lichen-size measurements at a few control sites is valid on a regional scale. Our scope also includes the importance of site selection, identification of significant peaks in probability-density distributions of lichen sizes, calibration of distinctive phases of lichen growth, and applications of the coseismic rockfall model. Discussion follows the flow chart of Figure 2. Event ages are purposely stated in terms of lichen size, because age estimates may change with improvements of the lichen-growth equation. We conclude that this versatile approach to lichenometry can produce precise age estimates for geomorphic events in many mountainous regions.

COSEISMIC ROCKFALL LICHENOMETRY MODEL

New Zealand is well suited for development and testing of the coseismic rockfall lichenometry model. Large earthquakes capable of causing regionally extensive rockfalls have occurred throughout the Southern Alps. Most earthquakes are widely spaced in time relative to the moderately rapid growth of the lichens used in this study, *Rhizocarpon* subgenus *Rhizocarpon* (collectively referred to as yellow rhizocarpons). Unstable outcrops of fractured graywacke sandstone on rugged mountainsides ensure an ample supply of blocks for talus and debris slopes. Steep hillsides underlain by hard, brittle graywacke typically fail by rockfall and rock-avalanche processes (Whitehouse, 1983). Fresh substrates for new lichens—outcrop joint faces as well as rockfall blocks—may be created by rainstorms, freezing of water along joints and fractures, pas-

sage of animals, avalanches, and wedging by roots and soil. These processes loosen blocks that tumble downhill during times of seismic shaking. Each rockfall block may have a different history of detachment from an outcrop, episodic travel downhill, local microclimates, and colonization by primitive plants.

Regional Rockfall Events

Earthquake-induced landslides are widespread and common in many alpine mountains. Earthquakes with Mw magnitudes greater than 7 can trigger rockfalls at distances of up to 400 km from their epicenters (Keefer, 1984, 1994; Wieczorek et al., 1992; Wieczorek and Jäger, 1996). Mw refers to the seismic-moment magnitude scale as defined by Hanks and Kanamori (1979). A coseismic landslide is a mass wasting event triggered by, and therefore occurring during or shortly after an earthquake. Lichens have been used to date rockfalls (Porter and Orombelli, 1981) and coseismic landslides (Smirnova and Nikonov, 1990). A coseismic rockfall event is distinctive. It occurs at many sites throughout a region (Fig. 3), and rockfall abundance increases toward the earthquake epicenter. Coseismic rockfall events can be dated by measuring sizes of lichens with systematic growth rates that colonize the newly exposed rock surfaces (Bull et al., 1994; Bull, 1996a, 1996b).

Moderate earthquakes (Mw = 5.5 to 7), such as the Mw 6.1 Tennyson earthquake of 1990 in our study area, are accompanied by clouds of dust caused by abundant rockfalls near their epicenters. Newly arrived blocks in rockfall deposits are distinctive because their freshly exposed surfaces have no lichens. Fresh rockfall blocks are common only within 15 km of the 1990 earthquake epicenter.

Coseismic events dominate the rockfall process in much of the Southern Alps. Many sites where the largest lichen on each block is at least 8 mm (Fig. 4) are indicative of rockfall deposits that have not received an increment of new blocks since the Inangahua Mw 7.1 earthquake of 1968 (Downs, 1995).

Hillslope processes are so active in the Southern Alps that many lichenometry sites only record rockfalls of the past 500 yr (~85 mm); 1000-yr-old rockfall blocks (~165 mm) are rare. The time span of rockfall events that can be dated using lichenometry is influenced by the frequency of reworking of the rockfall deposit. Some blocks are broken or partially covered by incoming new blocks, and fresh substrates are colonized by new lichens when blocks are overturned or when adjacent soil or rock detritus moves downhill. Additions and redistributions continue until few old blocks remain, their largest

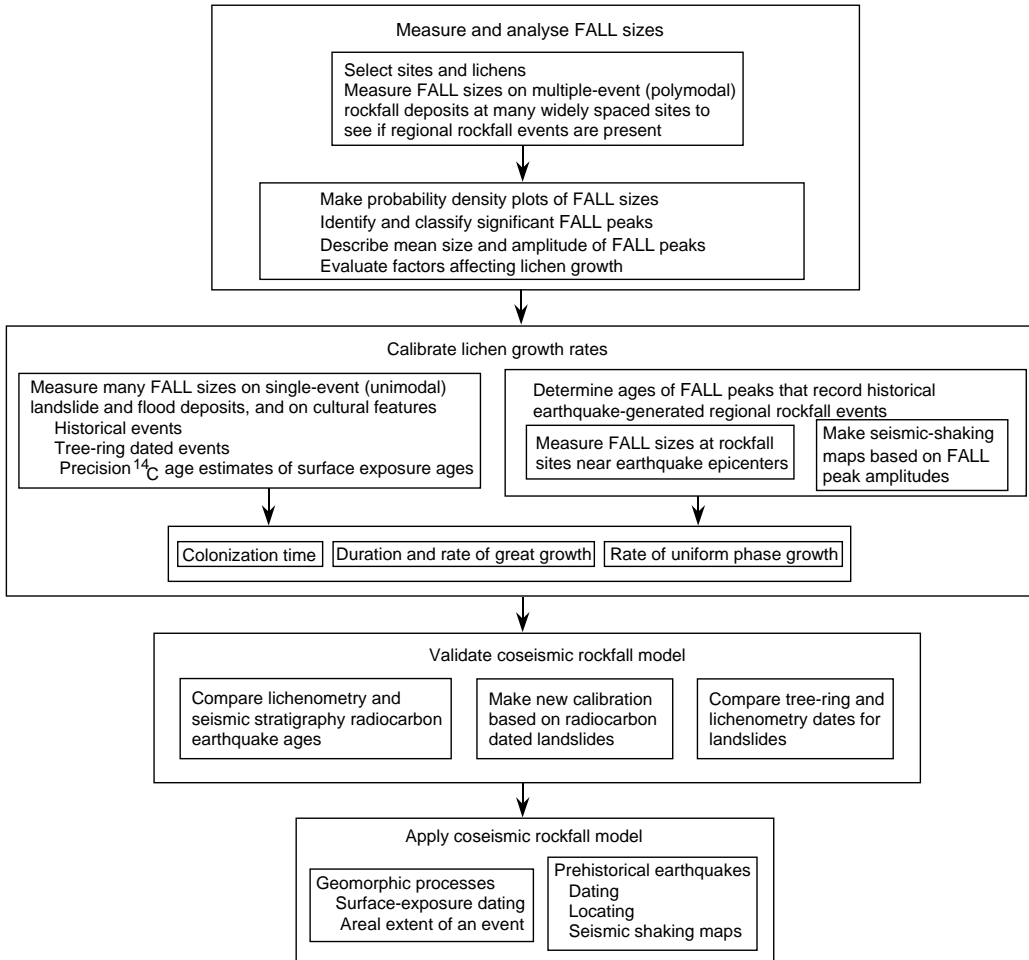


Figure 2. Flow chart showing the method, validation, and applications of the coseismic rockfall lichenometry model. The acronym FALL stands for “fixed-area largest-lichen” and indicates measurement of the size of the largest lichen within a fixed sampling area.

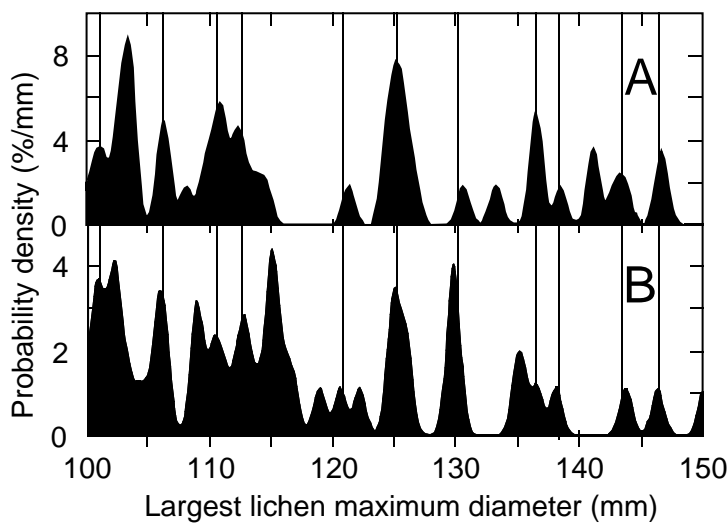


Figure 3. Probability density plots for FALL sizes for *Rhizocarpon* section *Superficiale* growing on rockfall blocks derived from late Holocene glacial moraines near Mount Cook. Vertical lines denote FALL peaks for regional rockfall events that occurred at both sites. The 108, 115, and 135 mm rockfall events at the Celmisia site occur at other sites in the study region. The 125 mm regional rockfall event is strong typically in a 400 km long area east of the crest of the Southern Alps (Bull, 1996a). Density plots were constructed using a Gaussian kernel size of 0.5 mm. (A) The Idyllic site is on a moraine of the Mueller Glacier; $n = 45$. (B) The Celmisia site is on a moraine of the Tasman Glacier; $n = 48$.



Figure 4. Accumulation of rockfall blocks on a stream terrace at the No Man's Creek site. FALL sizes range from 8 to 104 mm. Person is standing by a light-toned block with 8 mm lichens that date to 1968. Impact marks leading to the 1968 blocks are still present on the hillslope above the rockfall deposit.

lichens documenting only the largest of the old rockfall events.

FALL Method

Landslide, stream, shoreline, and glacial and periglacial deposits commonly have enough cobble- and boulder-size blocks to allow a sampling strategy that we refer to as the fixed-area largest-lichen (FALL) method. FALL size is defined as the maximum diameter of the largest thallus, black prothallus rim included, found in a unit sample area. The contrast between the conventional and FALL methods for lichenometry can be illustrated by considering a population of lichens growing on a recently exposed, glacially polished rock surface. The conventional method would use the largest lichen, or mean of five largest lichens measured in a 1 hr search. The FALL method would measure the longest axis of the largest lichen in each of 100, or more, sample areas of about the same size (for example, 1 m²). The FALL method averages out the effects of locally variable colonization times and growth rates, taxonomic misidentification, inherited lichens that predate the surface we seek to date, and lichens that have merged to form composite thalli. Note that we use an informal terminology, referring to FALL distributions and FALL peaks to avoid more cumbersome terms such as FALL-size distribution and FALL-size peak.

FALL measurements are best displayed using a probability density plot (e.g., Fig. 3). The prominent peaks in the FALL distribution are viewed as a record of short-lived events that caused reworking of parts of the deposit. Probability density is everywhere normalized to the same units, percent per millimeter, to facilitate comparisons between density plots.

The ideal lichenometry sampling strategy should attempt to minimize inherent measurement variability by considering sample area (Innes, 1984, 1985a; Spence and Mahaney, 1988) and density of lichen thalli. The ideal data set would result from a sampling strategy that measured the largest isolated lichen in a number of fixed-size sampling areas where conditions for colonization and growth were identical but the areas were otherwise independent of each other.

Our lichenometry sites depart from this ideal strategy, because our unit sampling area was allowed to vary as a function of block size. Block diameters are generally in the range of 0.2 to 1 m, and the viable surface area for lichen growth ranges from 0.04 to 1 m². For cool, humid New Zealand, yellow rhizocarpons prefer the top and north sides of blocks, which are relatively sunny and dry. We tried to confine our measurements to these exposed surfaces to reduce variations in colonization time and growth rates.

Mosaics of intergrown lichens are rare at our sites, but some largest lichens were not measured

because growth of their longest axis was constrained by adjacent yellow rhizocarpons. Isolated lichens are less common on old blocks, so our FALL distributions undersample old thalli. Burial of old blocks by younger blocks also reduces opportunities to measure lichens associated with old rockfall events.

The FALL method also works well for lichens growing on joint faces of outcrops from which the rockfall blocks are derived. Typical joint faces in fractured graywacke are 0.03 to 0.2 m², which are smaller in area than most blocks in our rockfall deposits.

Site Selection

Selection of lichenometry sites has a crucial influence on precision of age estimates and resolution of closely spaced events. Factors to consider in site selection include diversity and frequency of geomorphic processes, lichen species and abundance, quality of thalli, substrate smoothness, sizes of rockfall blocks, and ability to recognize old, stabilized block fields where lichen communities are not related to the times of substrate exposure because the first generation of lichens has died and has been replaced.

Diverse landforms may generate, or intercept and store rockfall blocks. Examples include hillslope benches and concave footslopes, ridgecrest saddles, stream terraces, alluvial fans, and glacial moraines. Paleoseismologists generally seek rock-

fall sites that are sensitive to seismic shaking, such as steep hillsides, bouldery glacial moraines, and rock avalanches with minimal fine sediment. Seismic shaking is more likely to affect a young unstable deposit than an older more stable deposit.

Rockfall deposits accumulate incrementally during times of seismic shaking and storms, or as random rockfall events. Blocks detached from outcrops are spread across the surface of talus or debris slopes. Rockfall blocks derived from part of a cliff disperse as blocks strike each other, lower outcrops, and talus-, debris-, or snow-covered slopes. Rapp (1960, Fig. 11) documented the routes traveled by 34 disk-shaped rockfall blocks of mica schist at Kärkevagge in northern Sweden. They dispersed into a 170-m-wide swath while traveling 150 to 400 m horizontally and 120 to 220 m vertically. The end product of repeated outcrop collapse is a highly diachronous block field, where overall ages and sizes of rockfall blocks increase downslope (Whitehouse et al., 1983).

The dominant geomorphic process partly determines the usefulness of lichenometry sites in alpine mountains. Debris and talus cones below chutes and ravines generally should be avoided, unless one wants to study frequency of snow avalanches and debris flows triggered mainly by nonseismic events. Planar sheets of talus whose blocks are derived from the triangular facets between chutes or stream channels may contain a more reliable paleoseismic signal because rockfalls may be the dominant process. Moraines generally lack the height needed to be a source of avalanches, and rainstorm-induced landslides are not likely to occur in moraines consisting of permeable gravel.

Old stabilized block fields, on which several generations of lichens have grown and died, generally have minimal geochronologic information. Such blocks may have weathered surfaces or may be largely buried by fine detritus. Such sites typically have slopes that are much less than the angle of repose for talus. Nearly circular, isolated lichens are suggestive of a first-generation lichen community. Blocks whose oldest lichens colonized long after the time of initial substrate formation typically have large thalli with highly irregular margins, or the lichens may have grown together to form a mosaic of thalli margins. Block fields that accumulate slowly may have a mixture of datable and undatable blocks, and should be avoided.

Paleoseismologists may select sites with different sensitivities to seismic shaking in order to identify the fault responsible for a prehistorical earthquake (Bull, 1997). Potential sites, listed in order of increasing sensitivity to seismic shaking, are:

Massive outcrop with few visible joints.

Fractured outcrop.

Fractured outcrop with prominent joint sets that are vertical and parallel to the hillside.

Fractured outcrop with multiple joint sets undercut by fluvial, glacial, or shoreline erosion.

Fractured surficial blocks on the distal ridge of a rock-avalanche deposit.

Steep-sided young glacial moraine.

Riser of stream terrace in sandy gravel.

Top of barren talus cone at the angle of repose.

Block size influences survival of lichens. Tops of large blocks are more fully exposed to sunlight and less affected by fire. Large blocks are less likely to be buried or overturned but are more likely to be struck by subsequent rockfalls. But working on blocks larger than 3 m is time consuming and can be hazardous.

True linear distances are preferred for lichen-size measurements. Substrates with smooth planar joints, such as quartzitic sandstone and fine-grained plutonic rocks, provide reliable digital-caliper measurements. Approximate sizes of lichens growing on highly curved river or beach cobbles can be estimated with a flexible ruler. Lichens growing on rough rock surfaces, such as highly fractured argillaceous sandstone or porphyritic plutonic rocks may yield unreliable measurements. The best measurements are made on lichens growing on smooth surfaces. Rough surfaces or lichens growing across steps greater than 1 mm should be avoided.

The ideal coseismic rockfall lichenometry site is sensitive to both nearby and distant earthquakes. Such a site would have:

Unstable cliffs of fine-grained, strongly jointed rock.

Pervasive joints that parallel the cliff face.

Abundant blocks with smooth planar surfaces.

A limited size range for most blocks (such as 0.5 to 2 m).

A large repository of blocks close to the angle of repose.

Extensive, thick deposits of blocks devoid of plants, which might shade lichens or provide fuel for fires.

A local microclimate that favors the species of lichen being measured and that lacks persistent snow cover, which can kill lichens.

Lichen Selection and Quality

Slow-growing lichens are preferred for dating old geomorphic events, whereas fast-growing lichens are useful for precise dating of young, closely spaced events. *Rhizocarpon* subgenus *Rhizocarpon* are the slowest growing New Zealand lichens. The moderately slow growing *Rhizocarpon candidum* is a white lichen with excellent quality thalli (Burrows et al., 1990).

A quality assessment was made with each lichen-size measurement. Assigning general

classes of thallus quality identifies the lower limit of acceptable lichen-size measurements and is a numerical way of identifying sites with favorable lichen characteristics. Quality 3 is average, 1 is exceptionally nice, and 4 is barely good enough to include in a data set. The thallus quality number was appended to each measurement. For example, the 2 in 35.672 records an above average quality for a lichen whose digital caliper size was 35.67 mm. Noncircular habit, irregular margins, slight fuzziness of the prothallus rim at the measuring points, or a nonplanar substrate result in a lower quality rating. Thallus-quality rating is raised by 1 when several of the largest lichens on a block are about the same size. Thallus quality in our study area is fairly typical of yellow rhizocarpons, being mainly class 3 with common class 4 and class 2 lichens; class 1 is rare. We have noted that the widths of FALL peaks increases with decreasing lichen quality. All four classes of lichen quality were included in the data sets, because our perception is that peak means are not affected by lichen quality even though variance of the measurements is.

A few blocks on glacial moraines, landslides, and debris-flows may be derived from sources whose lichens predate the deposit being dated. Identification of these inherited lichens commonly is subjective. The objective approach used here is to measure all appropriate largest lichens, including those that may appear anomalously large or small. We assume that inherited lichens are rare and that they will tend to be incorporated into the high-side tail of the FALL distribution. They should not significantly affect the means of FALL peaks. These assumptions can be validated by comparing FALL peaks at several sites.

Several assumptions pertain to our measurements of FALL sizes: The largest lichen on the block was the first to colonize the rockfall block. Lichen growth has been unconstrained. The rate of growth is similar to the average for yellow rhizocarpons.

Important subjective decisions include:

1. Is the lichen a single thallus or a composite? This crucial evaluation is easy for a thallus with concentric rings of areoles, or where black prothallus rims indicate obvious merging of thalli. All gradations exist, so the composite nature of other thalli may go unrecognized.

2. Are the margins, long axis, and degree of circularity of the thallus of sufficient quality to warrant inclusion in the data set?

3. Is the substrate sufficiently smooth and planar to permit a precise measurement?

Large sample sizes reduce the significance of these assumptions and decisions for any single thallus. We prefer samples of at least 50 measurements per rockfall deposit.

Digital Caliper Measurements

Some previous studies used dial calipers (Matthews, 1974; Innes, 1985a, Bickerton and Matthews, 1992), and Innes (1986) noted that calipers increase the precision of measurements made by different observers. Most lichenometrists use flexible plastic rulers and templates to measure lichens (Locke et al., 1979; Innes, 1985a; Winchester and Harrison, 1994). Assuming a ± 1 mm reading, ruler measurements degrade lichen-size measurements and the lichenometry age estimates, especially for slow-growing lichens. Digital calipers are clearly preferred for both precision and ease of use. They also help reduce unintentional measurement bias. An observer making ruler measurements is aware of the reading while placing the ruler on the lichen, and must round to the nearest millimeter. An observer making digital-caliper measurements is not aware of the lichen size until she or he looks at the readout. Evaluation of lichen quality continues during the process of carefully positioning the caliper blades at the endpoints of the longest axis. There is no need to look at the digital readout if one sees a fuzzy margin at either endpoint selected for measurement, or if at the last moment the observer recognizes coalescence of thalli. Bias is also reduced by assigning the lichen-quality number before looking at the readout, and by never deleting a measurement after looking at the readout of lichen size. Data loggers further reduce potential for bias, because the observer need not know any of the lichen sizes until the data set is downloaded into a computer.

Determining the largest of several lichens on a block is simple with digital calipers. After measurement of the apparent largest lichen, the caliper blades are placed on the longest axes of other possible largest lichens. It is easy to recognize both the largest lichen among several of about the same size and the longest axis of the lichen to be measured.

Precision and Replication. Reproducibility of measurements is influenced by instrumental and observer errors. Replicate measurement pairs are routinely within ± 0.20 mm of each other. A made-at-same-time replication error of ± 0.20 mm, or better, is attainable for >95% of the quality 1 or 2 lichens, 80% to 90% of the quality 3 lichens, and about 70% of the quality 4 lichens. Multiple measurements of a thallus diameter indicate that operator errors are very low (Table 1). Standard deviations of repeated measurements of a single lichen (about 0.06 mm) are larger than the manufacturer's estimates of instrumental error (0.01–0.02 mm) and are caused by the observer's inability to repeatedly place the caliper blades at exactly the same endpoints. In Test D of Table 1, fastidious cleaning and light lubrication

of the caliper and having one's hands comfortably braced decreased the variation of sizes from 0.26 mm to 0.17 mm and the standard deviation from 0.06 to 0.04 mm.

It would be useful to know whether, after an absence, an observer selects the same lichen on a rockfall block and the same long axis. Figure 5 shows the results of an experiment where replicate FALL measurements were made on marked blocks at several sites, with the pair of observations separated by an interval of 1 to 104 days. Measurement errors show no obvious correlation with lichen size. The distribution of paired differences is Gaussian and has a zero mean and a standard deviation of 0.66 mm. From this, we can estimate the standard deviation of a single

measurement, 0.47 mm ($0.66 \text{ mm} \times 2^{-0.5}$), given that replicate measurements have the same expected value and standard deviation but are otherwise independent. This single-measurement standard deviation represents the variation due to measurement errors alone. Errors increase slightly when a different observer makes the second measurement.

Our conclusion is that digital calipers can reduce measurement errors to an insignificant level, especially in the context of normal lichen growth. New Zealand yellow rhizocarpons have a growth rate of 1 mm every 6 yr during the uniform-growth phase. The measurement-related standard deviation of 0.47 mm is equivalent to a variation of 2.8 yr.

TABLE 1. REPLICATION MEASUREMENTS MADE WITH TWO DIGITAL CALIPERS ON DRY AND WET YELLOW RHIZOCARPONS

Test	Count	Minimum size (mm)	Maximum size (mm)	Mean size (mm)	Standard deviation	Standard error
A*	107	9.18	9.44	9.28	0.06	0.01
B†	53	9.18	9.38	9.28	0.05	0.01
C‡	59	9.17	9.44	9.28	0.06	0.01
D#	252	36.47	36.64	36.56	0.04	0.002

*Caliper 7123707, dry lichen, minimal operator experience.

†Caliper 7123844, on test A dry lichen.

‡Caliper 7123844, on test A lichen after wetting.

#Caliper 7123707, dry lichen, experienced operator.

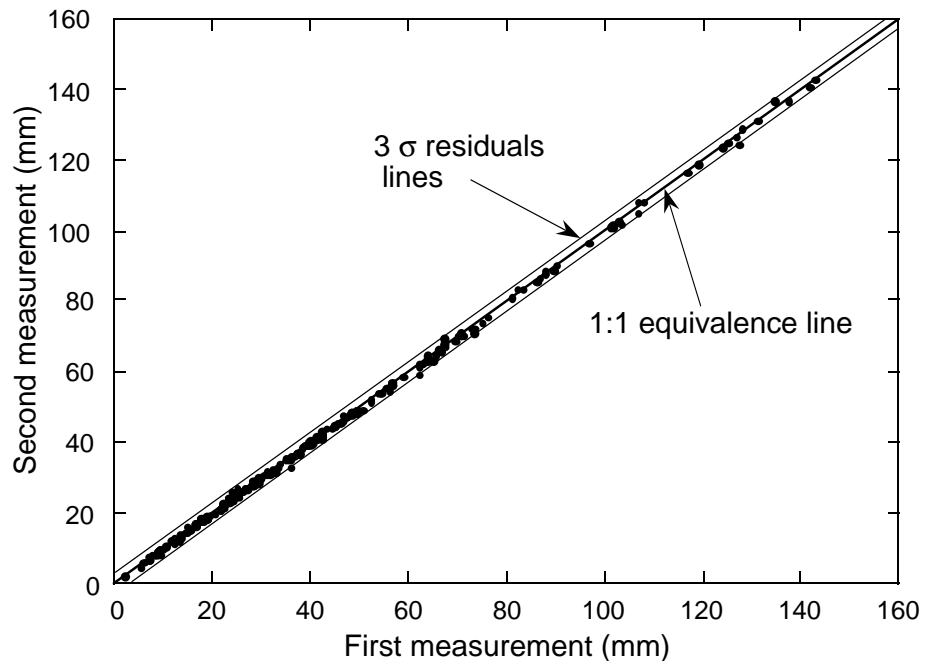


Figure 5. Comparisons of 243 replicate FALL measurements ranging from 2 to 143 mm. Approximately 90% of the replicate measurements were within 1 mm of the original, 74% within 0.5 mm, and 48% within 0.25 mm.

Single-Event and Multiple-Event Data Sets.

Our experience indicates that FALL distributions for single-event deposits have large standard deviations (e.g., glacier-outburst flood deposit of Fig. 6C), compared to the narrow peaks that are typical of a multiple-event rockfall deposit (Fig. 3). Our measurement standard deviation for a single lichen measurement is ~ 0.47 mm. So, the within-peak variation displayed in the FALL distributions (e.g., Fig. 6) must be due to natural stochastic processes related to colonization, growth, interactions with other lichens, and microclimate.

Single-event FALL distributions are typically unimodal with a bell-shaped form. All of the Figure 6 distributions, except for Figure 6A, are significantly different from Gaussian as judged by the χ^2 test (Press et al., 1992, p. 614). But the F test (Bevington, 1969, p. 200) indicates that the distributions are better fit by two superimposed Gaussian distributions. In other words, the tails of each distribution are longer than would be expected for a single Gaussian distribution.

Superimposed Gaussians are used to represent distributions where multiple stochastic processes introduce distinctly different magnitudes of variability to a distribution (Titterton et al., 1985, p. 22). For example, variations in colonization time will result in a Gaussian distribution with a relatively small standard deviation, but spatial variations in local microclimate might introduce relatively large variations in the growth rates of individual lichens. Variations in sample area from block to block add another source of variation to our data. Nonetheless, when analyzing our FALL distributions we assume that individual peaks can be represented by a single Gaussian. As a result, we are ignoring the stochastic processes responsible for the long tails of the FALL peaks.

Multiple-event FALL data sets are characterized by overlapping peaks (Figs. 3, 8, 12A, 13, and 15). Strong peaks are usually readily identified, moderate peaks may appear only as shoulders on the stronger peaks, and weak peaks may not be apparent at all.

The overall skewed shape of a polymodal FALL distribution provides information about the life-expectancy of the entire lichen population. For instance, the distribution for the Zig Zag site (Fig. 7) shows that older lichens with sizes of more than 40 mm are dying at a fast rate, presumably due to intermittent destruction of old blocks, and increasing competition for dwindling growth space. The oldest lichens, with sizes of about 135 mm, are rare and are estimated to be about 800 yr old.

FALL Peaks

Identification of Significant Peaks. Detection and resolution of FALL peaks and precision of lichenometry ages generally improves with

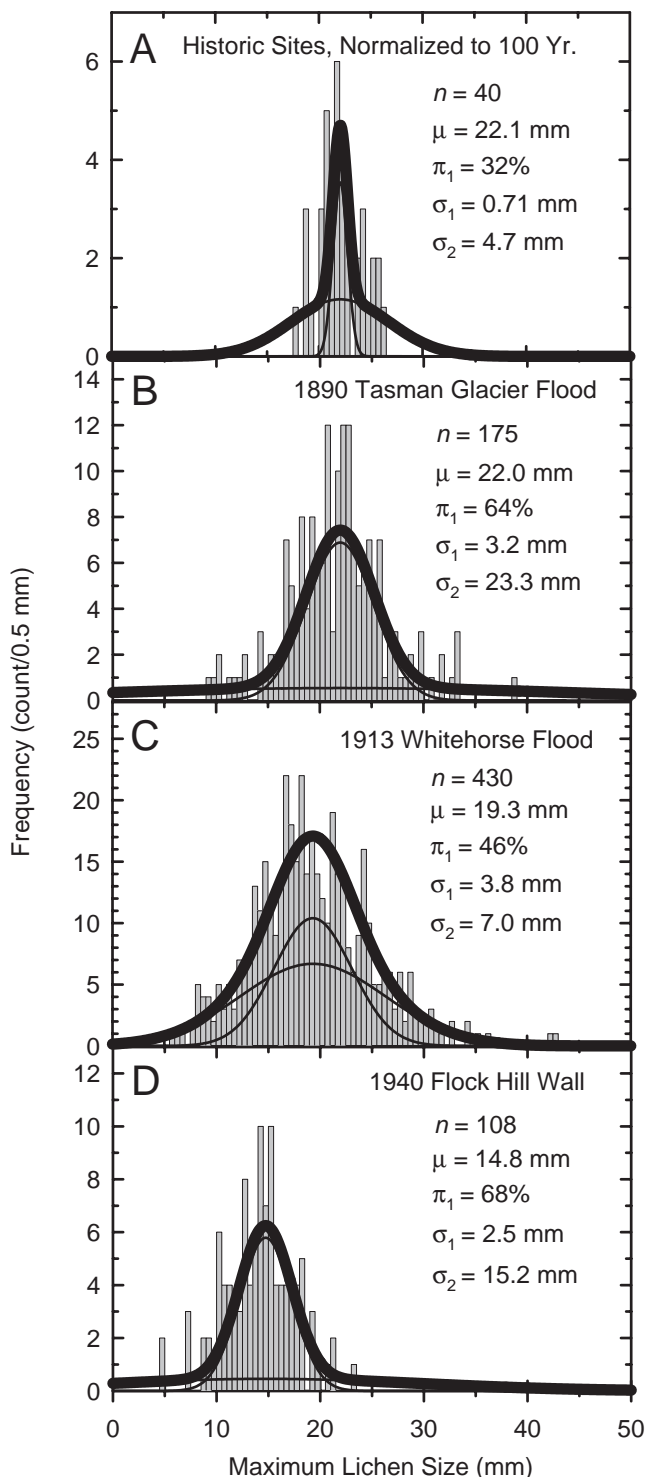


Figure 6. FALL distributions for single-event deposits. Each distribution is best represented by two superimposed Gaussians with different standard deviations (σ_1 , σ_2) and a common mean (μ). The parameter π_1 indicates the fraction of the total distribution included in the first Gaussian (μ , σ_1); n is the sample size. (A) Individual FALL measurements for historical stone structures of various ages. The FALL sizes were transformed to a single-age population of 100 yr using equation 10. (B) 1890 Tasman Glacier outburst flood deposits; $n = 175$. (C) 1913 Mueller Glacier outburst flood deposits near Whitehorse Hill. FALL measurements made by William Phillips and Nancy Sprague; $n = 430$. (D) 1940 wall at Flock Hill (Fig. 14); $n = 108$.

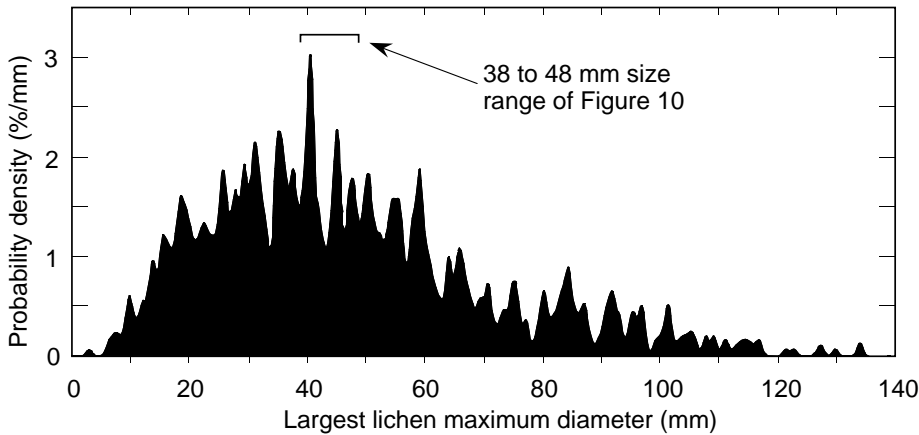


Figure 7. Polymodal, skewed FALL distribution for yellow rhizocarpons on historical (<30 mm) and prehistorical rockfall blocks at the Zig-Zag site. Gaussian kernel size is 0.5 mm; $n = 1151$.

increasing size of the data set. Small data sets reveal only the largest peaks. Thus, large data sets are required for confident identification of FALL peaks associated with weak or distant earthquakes. Essential supporting evidence for the coseismic origin of a FALL peak is the recognition of coeval peaks at multiple study sites. Regional-scale coverage increases the odds of detecting related peaks at multiple sites. This section examines resolution for different sample sizes, defines peak significance, and outlines criteria for weak, moderate, and strong classes of regional rockfall events.

Consider the general case of a histogram showing n measurements with FALL size indicated by D . The class interval for the histogram is δ and the count for each histogram interval is given by $\phi(D)$. The probability density is

$$p(D) = \frac{\phi(D)}{n\delta}. \quad (1)$$

Based on the usual assumption that samples of ϕ drawn at D are approximately Poisson distributed [valid when the expected distribution of $\phi(D) > 9$; Taylor, 1982, p. 210], then the relative standard error (RSE) for $p(D)$ is approximated by

$$\text{RSE}[p(D)] = \sqrt{1/\phi(D)} = \sqrt{\frac{1}{p(D)n\delta}}. \quad (2)$$

Equation 2 shows the trade-off for a given sample size between detection and resolution. As δ is increased, $\text{RSE}[p(D)]$ will decrease, and our ability to detect changes in probability density will im-

prove. However, this improvement comes at the expense of a decrease in resolution because of the larger δ .

Equation 2 also indicates that an increase in n will bring a decrease in $\text{RSE}[p(D)]$. Precision and resolution can be improved by increasing the size of the data set, either by measuring more lichens at a site or by combining data from several sites. We have found it useful to use a normalized measure of size, which we call the mean data frequency, $f_m = n/R$, where R is the range of FALL sizes in the measured distribution (e.g., $D_{\max} - D_{\min}$). For example, a data set that had 1500 FALL sizes between 0 to 30 mm would have $f_m = 50 \text{ mm}^{-1}$. Our data sets have f_m ranging from 1 to 119 mm^{-1} .

Our strategy for detecting peaks is to use a uniform distribution of FALL sizes as a null hypothesis and to determine which parts of the observed distribution have densities different from uniform. In practical terms, this null case can be viewed as representative of a FALL distribution for lichens growing at a constant rate on blocks in a deposit fed by continuous rockfall events. The assumption of a constant growth rate is applicable for the uniform phase of lichen growth as defined in the following. If the distribution were uniform, then the expected density,

$$p_{\text{uniform}} = 1/R = f_m/n. \quad (3)$$

The relative standard error for p_{uniform} is

$$\text{RSE}[p_{\text{uniform}}] = \sqrt{R/\delta n} = \sqrt{1/(f_m \delta)}. \quad (4)$$

We adopt the convention of selecting d so that $\text{RSE}(p_{\text{uniform}})$ is set to 33 percent, which gives

$$\delta = 9 \frac{R}{n} = 9/f_m. \quad (5)$$

Given this convention, the ± 3 standard error (SE) variation of a uniform distribution should be confined to densities less than $(p_{\text{uniform}} + 3 \text{ SE}) = 2 p_{\text{uniform}}$. Thus, peaks that rise above the $2 p_{\text{uniform}}$ line would have densities significantly greater than uniform. In this sense, the reference line remains fixed at $2 p_{\text{uniform}}$, independent of n . An increase in n does buy a decrease in δ , which means an increase in resolution.

Daily increments of FALL measurements on rockfalls at the Cattle Gully site (Fig. 8) illustrate the trade-off between detection and resolution. Eight days of work resulted in a total of 1237 FALL measurements. The number of daily measurements varied considerably: day 1, 191; day 2, 296; day 3, 219; day 4, 59; and days 5 through 8, 472 measurements. In Figure 8, the entire data set is compared with that for day 2. Although both histograms have the same general shape, the full data set (Fig. 8A) provides greater resolution.

Another advantage of scaling the class-interval size is that the relative standard errors of the probability density estimates are stabilized. This relationship is illustrated in Figure 9, which compares replicate data sets for Cattle Gully. For this diagram, the histograms are plotted using points, and each point marks the top center of a histogram bar. The thick line shows the histogram for days 1–8, whereas the daily histograms, which can be viewed as replicate samples, are indicated by different point symbols. Equation 5 was used to determine the class interval for each histogram. The thin lines show the 2 SE range from equation 2 for the combined data (thick line). In almost all cases, the replicate data points lie within the 2 SE envelope. This result can be explained by substituting equation 5 into equation 2, which gives

$$\text{RSE}[p(D)] = \sqrt{\frac{1}{9p(D)R}}. \quad (6)$$

This relationship shows that the scaling introduced by equation 5 stabilizes the relative standard errors for the probability densities estimated by the histogram method so that they are independent of n . Using this procedure, an increase in n will improve the resolution between FALL peaks but not the precision of the probability density estimates.

Recognition of minor FALL peaks is crucial for detecting coseismic rockfalls over a broad area and for constructing peak-size maps. A seemingly minor peak in a FALL distribution needs to be

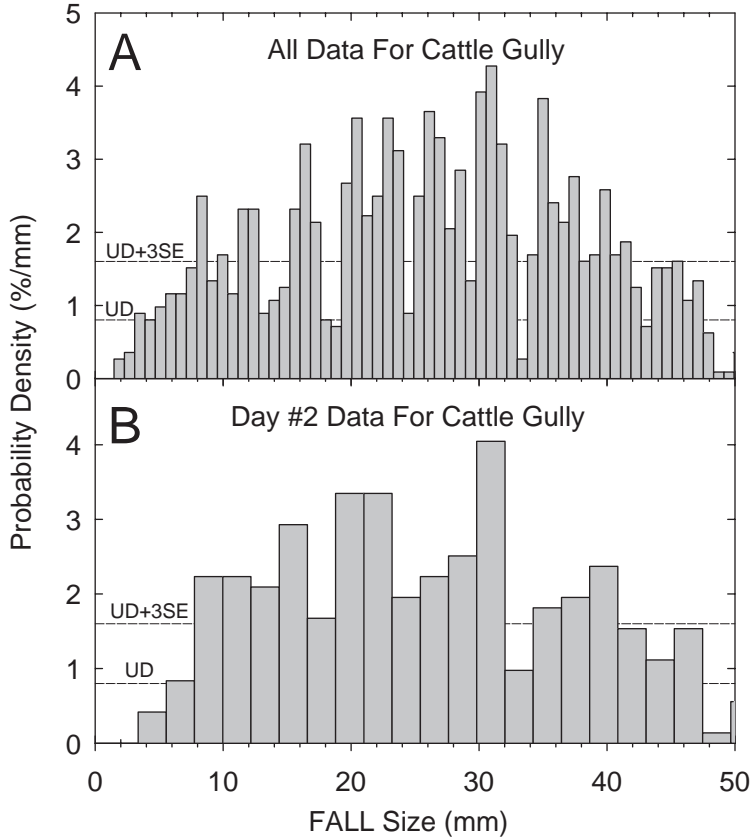


Figure 8. Comparison of histograms for different portions of the Cattle Gully data set; 1 to 48 mm size range. Precision (standard error) for the estimated probability density has been standardized for the two plots, using equation 5, by scaling the class interval relative to n . UD = expected density for a uniform distribution. UD + 3 SE = expected upper limit for random variations in density associated with a uniform distribution. 3 SE indicates three standard errors. (A) Days 1 through 8, $n = 1237$. (B) Day 2, $n = 296$.

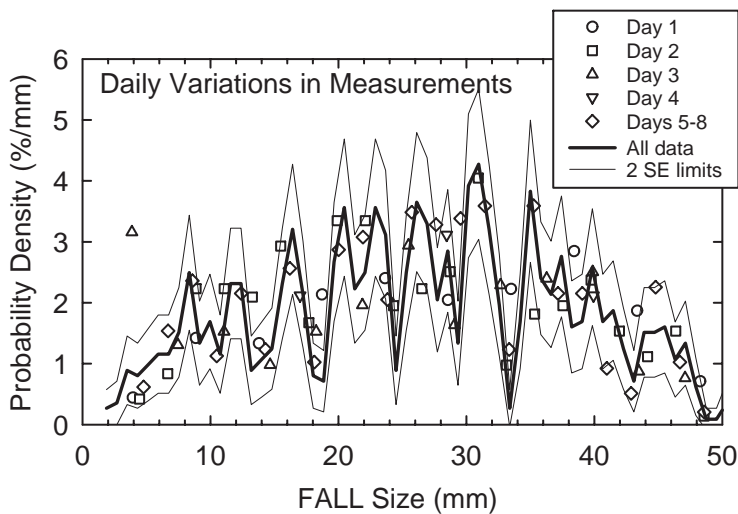


Figure 9. Probability density of 1237 measurements in the 1 to 48 mm FALL-size range at the Cattle Gully site, with two standard error confidence band. Density estimates for daily data based on equation 5 generally occur within the 95% confidence band for the entire data set.

identified as (1) a regional feature correlative to coeval peaks, both small and large, at other sites; (2) a local feature; or (3) statistical noise. Correlations between sites provide an essential test of our hypothesis that large earthquakes generate synchronous rockfalls at a regional scale. We recommend the following classification for regional studies with more than 20 lichenometry sites. FALL peaks are classed as regional if they are found at a minimum of three other sites. Peaks are termed weak if they rise 2 to 3 standard errors above the p_{uniform} line for a particular site or are present at only 20% to 40% of sites; moderate if 3 to 4 standard errors above p_{uniform} or present at 40% to 60% of sites; or strong if more than 4 standard errors above p_{uniform} or present at more than 60% of sites.

Probability Density Plots. Probability density plots provide another tool for analysis of FALL distributions. These plots are constructed by converting each measurement into a unit Gaussian function and averaging the densities of the overlapping Gaussians (Silverman, 1986, p. 15, 45; Brandon, 1996). The result is analogous to a histogram, but each observation is represented by a unit Gaussian instead of an increment of a histogram bar. Histogram class-interval size is replaced by a Gaussian kernel size, h , which defines the width of the unit Gaussian used in constructing the plot. The plot is given by

$$p(D) = \frac{1}{nh\sqrt{2\pi}} \sum_{i=1}^n \exp\left[-\frac{1}{2}\left(\frac{D - D_i}{h}\right)^2\right] \quad (7)$$

where D_i are the FALL measurements with $i = 1$ to n , and $p(D)$ is the probability density as a function of D for the entire FALL distribution. An advantage of the plot is that it provides a smooth and continuous display of the estimated probability density. The Gaussian kernel size h affects the degree of smoothness. Consider a single Gaussian peak with a standard deviation of σ . When viewed in a probability density plot estimated by the Gaussian kernel method, the peak will have an apparent standard deviation,

$$w = \sqrt{h^2 + \sigma^2}.$$

Therefore, as h increases, the apparent width of the peak, w , will increase, and adjacent peaks will merge together (See Brandon, 1996, for details).

Selection of an optimal kernel size must balance two competing objectives: to resolve closely spaced peaks and to guard against excessive random variations in density (i.e., noise) that might appear as real peaks. A practical estimate for the

optimal size of the Gaussian kernel is about 0.6 times the standard deviation of the measurement error (Brandon, 1996). For our case, this rule of thumb suggests $h \approx 1.5$ mm. The inference is that when h is set to less than this value, the density plot will contain significant noise. When h is greater than this value, peak resolution will be significantly degraded.

The large Zig Zag data set (mean data frequency, $f_m = 21 \text{ mm}^{-1}$) in Figure 10 illustrates the influence of kernel size on the estimated density plot for $h = 0.1$ to 2.5 mm. Also labeled are nine regional peaks that were found at three or more sites in our South Island study area. The density plot with $h = 2.5$ mm (Fig. 10D) fails to show any detailed structure because two real peaks have been merged into a single composite peak. The $h = 1.0$ mm plot (Fig. 10C) shows two strong peaks. The $h = 0.5$ mm plot (Fig. 10B) reveals a third strong peak at 47 mm and a modest shoulder at 42 mm. The $h = 0.1$ mm plot (Fig. 10A) shows all nine regional FALL peaks, but eight low amplitude peaks and three shoulders have also been introduced. The price of the extra resolution is extraneous noise. Additional work may show that some of the minor peaks belong in the regional category, or that some represent local events, but we suspect that many are related to noise introduced by a relatively small kernel size.

Density plots for this paper were prepared using kernels with $h = 0.1$ to 2.0 mm, depending on the size of the data set and the need to generalize or show details. Our experience indicates that $h = 0.1$ mm works well for data sets with $f_m > 20 \text{ mm}^{-1}$.

Like the histograms, uniform density can be used as a reference for the probability density plots. Equations 3.8 and 3.9 in Silverman (1986) were used to determine the expected mean and standard error for the density estimated by the Gaussian kernel method for a sample drawn from a uniform distribution. Given the reasonable assumption that $R \gg h$, then the expected value for p_{uniform} is

$$p_{\text{uniform}} \sim 1/Rh = f_m/nh \quad (8)$$

with a standard error of

$$SE(p_{\text{uniform}}) \approx \sqrt{1/nRh^2} = \sqrt{f_m/nh} \quad (9)$$

The upper limit of variation in the density for a uniform distribution would lie at about $p_{\text{uniform}} + 3 SE(p_{\text{uniform}})$. This limit is viewed as a rough indicator of the detection limit needed to separate real peaks from suspected noise. Once again, we have shown that detection of FALL peaks is improved by increasing n . Conversely, a decrease in h will make it more difficult to separate real peaks from statistical noise.

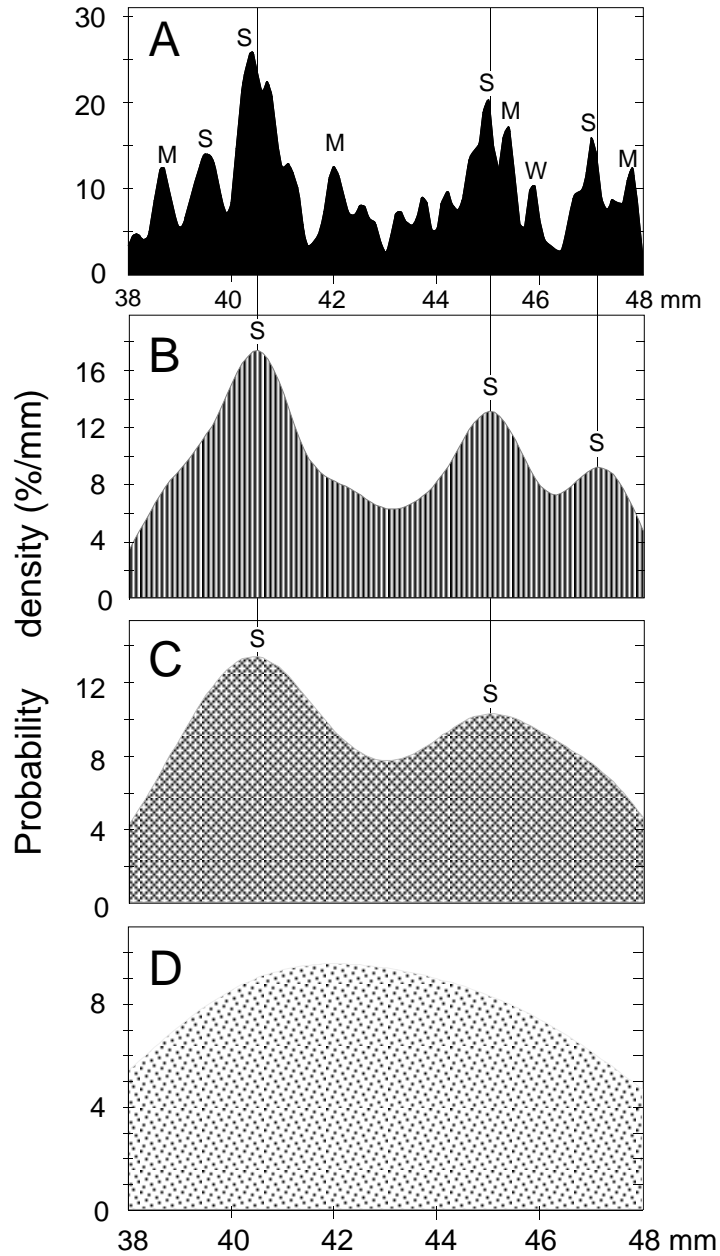


Figure 10. Effects of different kernel sizes (h in equation 7) on resolution and precision of FALL peaks in density distributions of 211 yellow rhizocarpons in the 38 to 48 mm size range at the Zig-Zag site. See Figure 7 for the full distribution. Gaussian kernel sizes of 2.5 (D), 1.0 (C), 0.5 (B), and 0.1 (A) mm result in progressively more detailed probability density plots. Strengths of significant peaks are noted as weak, W, moderate, M, or strong, S.

Mean and Size of FALL Peaks. The abundance of earthquake-generated rockfalls is a function of the intensity, direction, and duration of seismic shaking. Thus, a FALL peak resulting from a seismic-shaking event has a size that should scale approximately with the intensity of local shaking. Factors that affect coseismic rock-

fall production include the magnitude, distance, and propagation characteristics of the earthquake, amplification characteristics of seismic waves in local materials, topographic focusing of seismic energy, and outcrop resistance to seismic shaking. Fractured graywacke is the dominant rock type on the typically steep slopes of our

study area. Keefer's (1994) calculations for Peru indicate that 99% of the volume of coseismic landslides is caused by earthquakes larger than Mw 6, and 92% larger than Mw 7. Approximately 30 significant peaks are present in the FALL distribution for the Zig-Zag site (Fig. 7). All of these peaks are inferred to have formed during regional rockfall events because the peaks for these events are present at multiple sites. We interpret the peaks to be a record of at least 30 earthquakes with Mw > 7 during the past 800 yr.

We employed a commercially available computer program (PeakFit by Jandel Scientific) to estimate the mean, width, and size of FALL peaks in the density plots (see Figs. 11, 21, and 22). The general problem of fitting Gaussian peaks to density plots is discussed in Brandon (1992, 1996). The mean of the fitted peak is used to estimate the age of a rockfall event, whereas the peak size provides an index of the intensity of the event at each site. Peak sizes for older events are reduced due to reworking by younger events (Figs. 7 and 12A). This bias can be minimized by normalizing the peak size by the number of FALL measurements within a larger range around the peak. We use a ±3 mm range in constructing our peak size maps introduced below.

Data from the Rough Creek site (Fig. 11) provide an example of decomposition of a density

plot into component Gaussians. Two shoulders suggest a mixed distribution. Decomposition of the plot reveals at least three components. The dominant peak has a mean of 16.27 ± 0.04 mm (95% confidence level). A linear calibration curve introduced below indicates that the age estimates for the three peaks are close to the times of historical earthquakes in 1881, 1929, and 1968 (Table 2). The largest peak records the 1929 Arthur's Pass earthquake, with an epicenter about 25 km away. The two smaller peaks appear to record coseismic rockfalls associated with the 1881 Hurunui earthquake (epicenter 65 km away) and the 1968 Inangahua earthquake (epicenter 130 km away). Relative intensities, as represented by peak sizes, increase toward the earthquake epicenters (Figs. 3 and 11 in Bull et al., 1994). Decomposition of a 20-site regional data set yields the same FALL means for the three regional rockfall events as estimated from the small Rough Creek data set (Fig. 11).

FACTORS AFFECTING LICHEN GROWTH

Lichenometric ages commonly are estimated with minimal knowledge as to how lichen growth varies with local microclimate, altitude, temperature and precipitation, duration of snow cover, competition with other plants; or with substrate

characteristics such as smoothness, lithology, and degree of weathering. Intuition leads one to expect local variations in growth rates that would require a new calibration of lichen growth at every study site. Limited knowledge about the factors affecting lichen growth has also tended to undermine the credibility of lichenometry. We believe it is important to determine the extent of the region for which a particular calibration is valid. We examine here the effects of fire and prolonged snow cover that can kill many lichens at a site, the growth rates of different yellow rhizocarpons, the effects of variable microclimate at one site, and the variation in lichen growth rates at 20 sites with diverse macroclimates.

Snowkill and Firekill Events

Lichenometrists making earthquake studies should be aware that fires and perennial snowfields can kill lichens over a large area. The vulnerability of lichens to persistent snow cover is an asset for alpine climate studies (Benedict, 1990, 1993), but it can be problematic for studies of regional-rockfall events because climate changes can produce regional changes in the extent of perennial snow cover. Examples of snowkill events have been recognized in the high regions of the Sierra Nevada of California (Curry, 1969) and the Rocky Mountains of Colorado (Benedict,

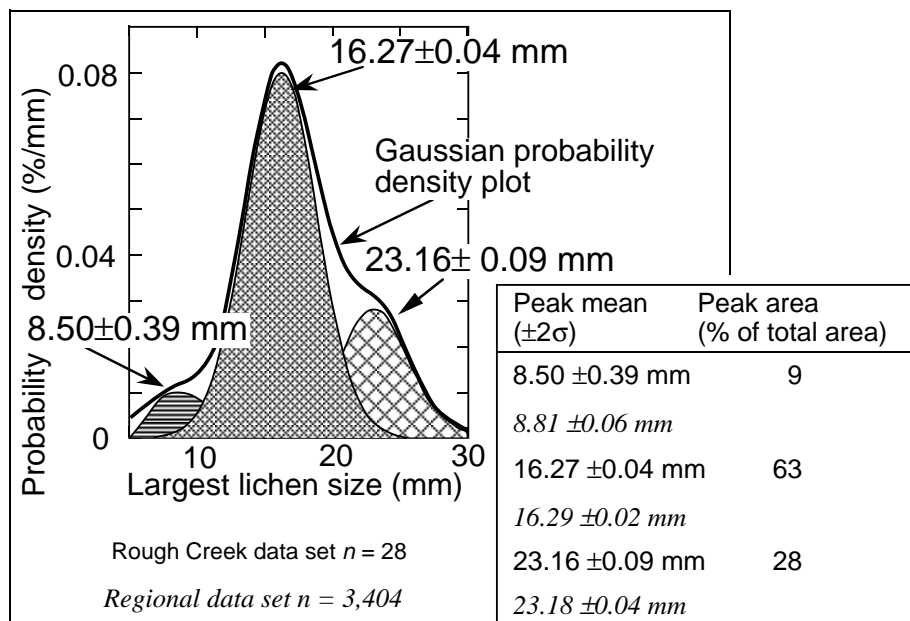


Figure 11. Decomposition of probability density plot of FALL sizes on historical coseismic rockfalls at Rough Creek. The density plot shows three peaks with mean sizes that are the same as for three regional rockfall events from the large Figure 15B data set. Kernel size is 0.5 mm; $n = 28$. Modified from Figure 2 in Bull et al. (1994).

TABLE 2. HISTORICAL EARTHQUAKES IN THE NORTHEASTERN PART OF THE SOUTH ISLAND OF NEW ZEALAND

Earthquake name	Main shock date	Approximate magnitude (Ms)
Arthur's Pass	1994.46	6.7
Tennyson	1990.34	6.1
Hossack	1973.31	5.5
Inangahua	1968.39	7.4
Acheron River	1960.14	5.4
Seaward Kaikoura	1955.45	5.1
Cheviot	1951.03	5.5
Waiau	1948.39	6.4
Lake Coleridge	1946.48	6.4
Arthur's Pass	1929.22	7.1
Murchison (Buller)	1929.46	7.8
Motunau	1922.98	6.4
Cheviot	1901.89	7
North Canterbury	1888.67	7.1
Hurunui	1881.93	>6.5
Nelson	1893.12	6.7
New Brighton	1869.43	5.7
Bealey	1866.08	>6.5
West Wairarapa	1855.06	8.2
Marlborough	1848.79	7.4

Note: Data taken primarily from Eiby (1968), Cowan (1989), Downs (1995), and Aitken and Lowry (1995). See Figure 1 for approximate locations of earthquake epicenters.

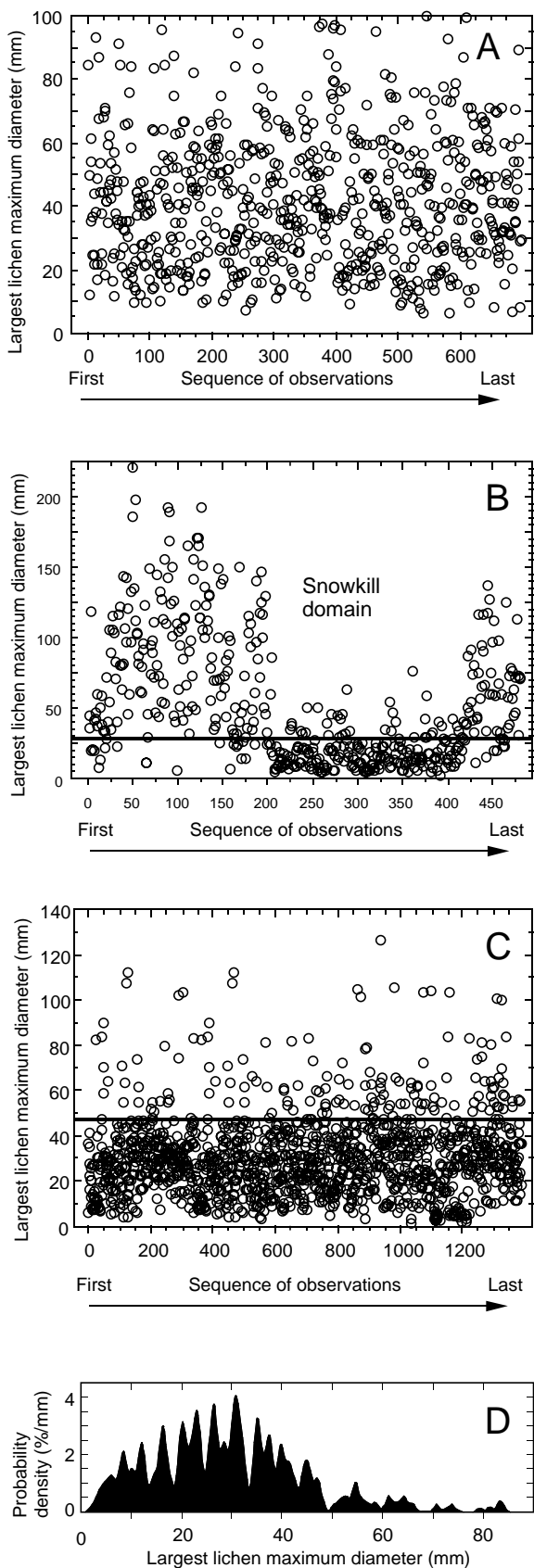


Figure 12. Evaluation of possible snowkill and firekill at lichenometry sites. (A) Univariate scattergram for traverse observations in the 0 to 100 mm size range at the Zig Zag site, altitude of 950 m. No obvious anomalies suggestive of either snowkill or firekill are present; $n = 692$. (B) Univariate scattergram of *Lecidea atrobrunnea* at the Chicken-foot moraine lichenometry site at an altitude of 3540 m in the Sierra Nevada of California. A domain of anomalous FALL density between observations 200 and 420 of the traverse suggests snowkill; $n = 481$. Tom Moutoux and Bill Phillips helped measure FALL sizes. (C) Univariate scattergram of *Rhizocarpon* subgenus *Rhizocarpon* for the Cattle Gully site, altitude of 500 m, reveals two domains of FALL densities above and below the 47 mm line, which dates a firekill event that removed many lichens; $n = 1388$. (D) Cattle Gully data shown as a density plot. The consequences of the firekill event can be seen as an abrupt transition to lower density of FALL sizes larger than 47 mm. Gaussian kernel size of 0.5 mm; $n = 1364$.

1990, 1993), at moderate altitudes in the Cascade volcanoes of Washington (Porter, 1981) where snowfields can persist for several years, and at low altitudes in the Arctic (Andrews et al, 1976; Williams, 1978; Koerner, 1980). Snowkill is not a problem at our New Zealand sites, which are at altitudes of only 380 to 1620 m, but firekill has occurred at a few sites.

Univariate scattergrams provide an easy way to detect the consequences of lichen-kill events. A scattergram is constructed by plotting FALL size as a function of observation number as one makes a sequence of lichen-size measurements while traversing a rockfall deposit. A deposit that accumulated during frequent events with approximately uniform dispersal to all parts of the deposit will have a scattergram that shows a similar pattern of FALL density across the entire traverse. For example, the density pattern of Figure 12A is characterized by uniformly scattered measurements between 10 and 60 mm and a gradual but systematic decrease in density above 60 mm. This decrease is attributed mainly to the removal of old lichens by death or burial and the introduction of younger blocks with fresh surfaces (also suggested by Fig. 7). In contrast, a snowkill or firekill event is revealed by a scattergram that has an abrupt decrease in density with increasing FALL size. The transition marks the time of the lichen-kill event.

The FALL distribution of Figure 12B illustrates a lichenometry transect on a glacial moraine in the Sierra Nevada of California that was affected by snowkill during the past 1000 yr. The density of the first 200 FALL sizes decreases gradually to 150 mm, above which lichens are sparse (much like the desirable situation portrayed in Figure 12A). FALL sizes at observations 200 to 420 in the traverse are much smaller; none are larger than 76 mm, and most are smaller than 28 mm. We infer a snowkill event immediately prior to 28 mm time (A.D. 1816 ± 10 yr). The high density of FALL sizes between 5 and 28 mm suggests that renewed colonization may have been restricted to local areas at first. The moraine may not have been entirely free of persistent snow cover until A.D. 1870 to 1915. This 19th century snowkill event is coeval with the Little Ice Age in the Sierra Nevada.

Our Cattle Gully site shows a good example of a firekill event. The scattergram (Fig. 12C) shows two density domains; the transition at 47 mm dates to about A.D. 1700. Pieces of charred, rot-resistant *Totara* wood on the Cattle Gully hillslopes suggest that fire may have killed many lichens, perhaps when Maoris used fires for clearing travel routes and flushing game (McGlone, 1979). The density plot (Figure 12D) shows that FALL peaks <47 mm were unaffected by the firekill event. For instance, the

31 mm peak was the result of a large nearby earthquake (Bull, 1997). The FALL distribution shows peaks >47 mm, indicating that some lichens survived the firekill event. Peakfitted means for this part of the distribution can be correlated with regional rockfall events, but the peak sizes have been so corrupted by fire damage that they cannot be used in peak-size maps.

Relative Growth Rates of Yellow Rhizocarpons

Taxa of New Zealand yellow rhizocarpons comprise several sections within the *Rhizocarpon* subgenus *Rhizocarpon* of the genus *Rhizocarpon* (Innes, 1985b). Each section of *Rhizocarpon* subgenus *Rhizocarpon* has many species. Laboratory identification of yellow rhizocarpon species (Benedict, 1988; Poelt, 1988) is time consuming and is not practical when measuring thousands of lichens. Instead, similar-appearing classes of bright greenish yellow lichens were distinguished in the field employing criteria similar to those used by Winchester (1989) and Werner (1990). Our field-based classifications were based on color, size, density and textural patterns of areola; size, morphology, and density of apothecia (reproductive structures); and width of prothallus rims. Representative samples were stained and studied with a binocular microscope by William Phillips (1993, personal commun.). Most keyed out as *Rhizocarpon* section *Rhizocarpon* and are presumed to represent several species.

FALL peaks for different types of lichens were compared to see if there were noticeable differences in growth rate. *Rhizocarpon* section *Superficiale* is a common lichen of good quality found on moraines (Fig. 3) in glacier forelands and on landslide deposits along the east side of the central Southern Alps (Burrows et al., 1990; Orwin, 1970). The good match of FALL peaks for *Rhizocarpon* section *Rhizocarpon* with those for *Rhizocarpon* section *Superficiale* (Fig. 13) suggests that visually different yellow rhizocarpons have similar growth rates, with one notable exception.

Rhizocarpon section *Alpicola* was measured only at the Otira Valley site and noted at the Ohau site; both sites are at relatively high altitudes (1300 m) and have extremely humid climates. Relative to sections *Rhizocarpon* and *Superficiale*, section *Alpicola* requires triple the colonization time, grows twice as fast during the great-growth phase, and has a slightly faster (105%) uniform phase growth rate (see the discussion of Fig. 18 below). These differences are enough to offset the FALL peaks for the *Alpicola* data set, relative to those for the other yellow rhizocarpons. Studies by Innes (1988) in southwest Norway also indicated a relatively longer colonization time followed by faster long-term growth rates for Section *Alpicola* (1985a, 1985c).

Microenvironment

Influence of local microclimate was assessed at a site with extreme contrasts. Vertical walls of stream-worn graywacke cobbles, held in place by wire mesh, were constructed in 1940 to protect a highway at the Flock Hill site. Common lichens in this valley-floor community are *Placopsis per-rugosa*, *Rhizocarpon geographicum*, *Parmelia adpicta*, *Placopsis parellina*, *Teloschistes velifer*,

Rhizocarpon sp., and *Lecidea* sp. (Orwin, 1970, 1971). Northwest-facing walls get full exposure to afternoon sun and to fierce northwest winds that descend the eastern slopes of the Southern Alps when storms pass to the south.

Sizes of yellow rhizocarpons were measured for each accessible cobble (unit sample areas were only ~0.01 m²) on the wall with the greatest microenvironmental contrasts (Fig. 14). Lichen cover in 1992 on the exposed north side was less

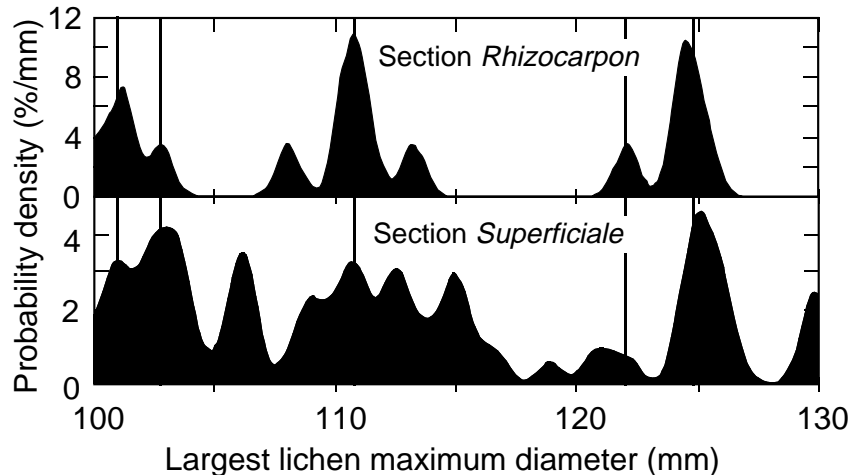


Figure 13. Comparison of FALL distributions for different large yellow rhizocarpons growing on rockfall blocks derived from late Holocene moraines of the Mueller (Idyllic site) and Tasman (Celmisia site) Glaciers near Mount Cook. Vertical lines denote FALL peaks for regional rockfall events that occur at about the same location in the distributions for two different Sections of *Rhizocarpon* subgenus *Rhizocarpon*. Gaussian kernel sizes are 0.5 mm; $n = 18$ and 74.

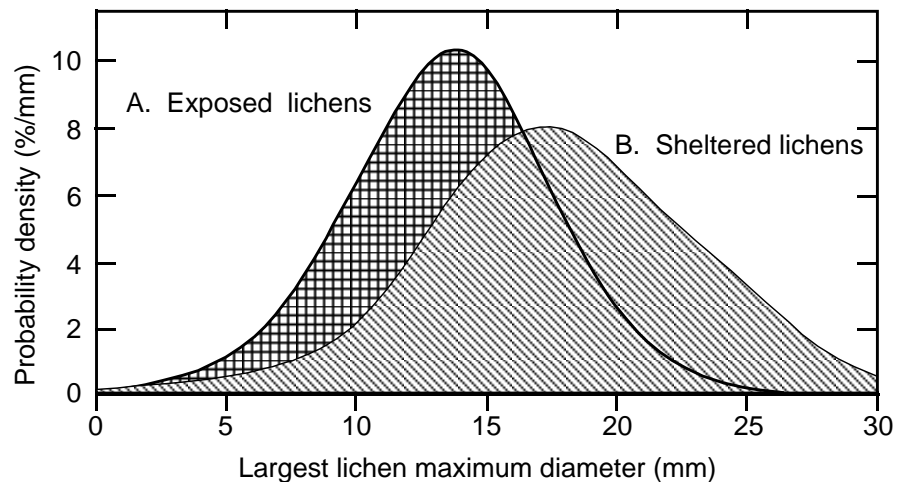


Figure 14. Microenvironmental control of lichen growth rates for yellow rhizocarpons growing on a wall. Plot A: lichens fully exposed to sunlight and gale-force winds; $n = 108$. Plot B: lichens sheltered from wind and afternoon sun; $n = 178$. Mean sizes of decomposed FALL peaks are 14.28 mm for Plot A, and 15.94 mm for plot B. Gaussian kernel size is 2.0 mm.

than 40%, and FALL sizes ranged from 4 to 23 mm. The cooler, wetter microenvironment of the sheltered southeast side also supported a few shrubs. Lichen cover was more than 80%, and FALL sizes ranged from 3 to 29 mm. Comparison of the peak means indicates about 20% faster growth for the sheltered lichens. Wider prothallus rims of lichens growing in sheltered microclimatic settings account for part of the size contrast. Our study supports Benedict's (1967) conclusion that shelter from sun and wind promotes faster growth of yellow rhizocarpons.

Complications caused by different growth rates in sheltered and exposed microenvironments were subsequently avoided by measuring only exposed lichens. The various genera of lichens on the rockfall blocks generally prefer specific exposure and moisture regimes (Jochimsen, 1973). Fortunately, New Zealand yellow rhizocarpons generally prefer the sunniest, driest parts of rockfall blocks. However, outcrops typically are shady and wet compared to rockfall blocks. Yellow rhizocarpons are not present on many outcrops, and where present, they are likely to grow in partially sheltered conditions. The apparently wider range of local microclimate for exposed yellow rhizocarpons that were measured on outcrops may explain their 2% faster growth rate relative to those growing on rockfall blocks (Bull, 1997).

Substrate Lithology and Altitude

We found yellow rhizocarpons on the following substrate lithologies: quartzitic graywacke sandstone, argillaceous and tuffaceous graywacke sandstone, andesitic basalt, syenite, quartz-biotite schist, and phyllite. Elongate lichens are more common on foliated rocks, but peak means are the same as those at nearby sites with nonfoliated substrate lithologies. Foliated rocks appear to constrain lichen growth only in the short axis direction. New Zealand yellow rhizocarpons have minimal differences in growth rates on noncalcareous substrates. A parallel conclusion was reached by Innes (1985c) in a study of lichen sizes on gravestones with diverse lithologies in Scotland.

The wide variation of climate present at the 90 lichenometry sites must be considered in the event that more than one calibration is required to define growth of *Rhizocarpon* subgenus *Rhizocarpon*. Study-site climate ranges from weakly seasonal humid to extremely humid, and from moderately seasonal mesic to frigid (classification of climate after Bull, 1991b, Table 2.1). Mean annual precipitation ranges from 700 to 5500 mm, mean January temperatures range from less than 12 to 15 °C, and mean July temperatures range from much less than 1 to about 4 °C (New Zealand Meteorological Service, 1985).

Precipitation, temperature, snow cover, and length of growing season are all factors that might affect lichen growth. All of these factors are strongly correlated with altitude. Thus, any relation between local climate and lichen growth rate should be revealed by examining lichen data sets collected at different altitudes. We combined data sets from 20 lichenometry sites with mean annual precipitation ranging from less than 500 mm to more than 5000 mm and a distribution of altitudes shown in Figure 15A. Regional variations in lichen growth rate would cause a broadening of the FALL peaks, but this is not apparent for the peaks in Figure 15B.

Thus we conclude that, with the exception of Section *Alpicola*, the growth histories and growth rates of many different species of New Zealand yellow rhizocarpons are remarkably similar, despite marked variations in altitude, local climate, and substrate lithology. Substrate-exposure ages can be estimated accurately using a single growth curve, because the data used to calibrate the curve are representative of yellow rhizocarpons of the study region. Other studies have also concluded that growth rate does not correlate with altitude (northern Sweden: Denton and Karlen, 1973; Bull et al., 1995. Sierra

Nevada of California: Bull et al., 1994). This conclusion does not indicate the absence of a climate effect. More likely, it means that the within-site variance for yellow rhizocarpon growth rate is significantly greater than the between-site variance caused by local climates. Note that yellow rhizocarpons in New Zealand grow one and one half times as fast as those in the Sierra Nevada, but only half as fast as those in Sweden. These intercontinental differences might be due, at least in part, to genetic differences that have evolved between these widely separated rhizocarpon populations.

PHASES OF LICHEN GROWTH

Lichens pass through three phases of growth—colonization, great growth, and uniform growth (Beschel, 1961; Innes, 1985a). Colonization is defined as the average amount of time between exposure of the substrate and the appearance of the first lichen. Colonization generally entails the delivery of spores to the substrate surface, the establishment of an initial symbiosis of the algae and fungi, and the growth of the nascent lichen to a visible size. Colonization time is expected to be a function of the area available for colonization.

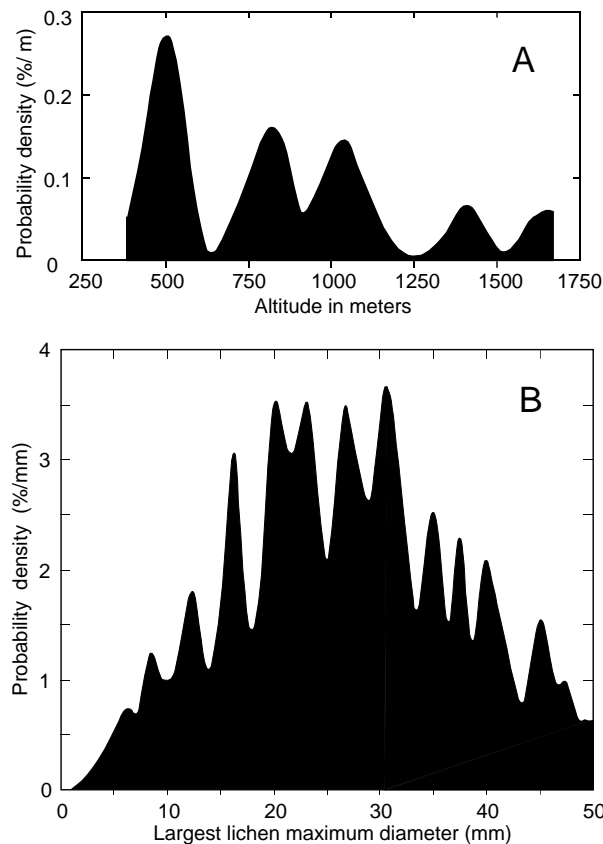


Figure 15. Probability density plots for combined data sets of 20 sites in 20 000 km² of the northern part of the South Island of New Zealand underlain by quartzitic graywacke sandstone, syenite, and argillaceous graywacke sandstone. (A) Site altitude ranges from 380 to 1620 m; Gaussian kernel size is 20 m. (B) Distribution of FALL sizes; Gaussian kernel size is 0.5 mm; $n = 5650$.

A larger surface should have a higher probability for receiving an initial viable spore in a shorter period of time, assuming that all other factors are equal. The strategy of using an approximately constant sampling area should help ensure that the time needed to colonize each block surface is, on average, the same. Yellow rhizocarpons on 12 year-old New Zealand substrates were large enough to be classed by Orwin (1970, 1971) as *Rhizocarpon geographicum* or *Rhizocarpon Superficialis*.

We introduce here a complete equation that incorporates the three basic phases of lichen growth,

$$D = D_0 \left(1 - e^{-K(\tau - \tau_0)} \right) + C(\tau - \tau_0), \quad (10)$$

where τ is the substrate-exposure age in years, and D is the size of the largest lichen on that surface in millimeters. The equation contains four parameters: τ_0 is the mean colonization time, K represents the nonlinear component of the growth rate during the great-growth phase, D_0 is the excess lichen size produced by great-growth, and C represents the constant growth rate during the uniform-growth phase.

Equation 10, as illustrated in the Figure 16, provides a complete description of all phases of growth. Calibration of equation 10 requires FALL data sets for substrates of known ages that cover both the great and uniform phases of growth. The Figure 16 analysis is based on data sets summarized in Table 3 and Figure 6. Historic stone structures, such as tombstones, provide 40 single observations (Fig. 6A). Large multiobservation data sets include the 1890 Tasman and 1913 Whitehorse glacier outburst floods and the cobbles in the 1940 Flock Hill wall (Figs. 6, B–D). Note that the peak means for the multi-observation data sets show much less scatter than that for the single-observation data because of the reduction in variance that comes with averaging the many lichen measurements in each multi-observation data set.

These data collectively define a growth curve for the past 150 yr. The parameters for equation 10 were estimated using standard methods for nonlinear least-squares estimation (Press et al., 1992). Weighting of the different types of data was accomplished by converting each FALL peak calibration point (Table 3) into a Gaussian-distributed set of FALL sizes with a mean, standard deviation, and count equal to the mean, width, and count of the FALL peak. The distributions were generated using the GASDEV routine of Press et al. 1992. Given this procedure, a single FALL measurement has unit weight, and multiobservation FALL peaks are weighted according to their peak size and peak width. The residuals after the regression indicate that the

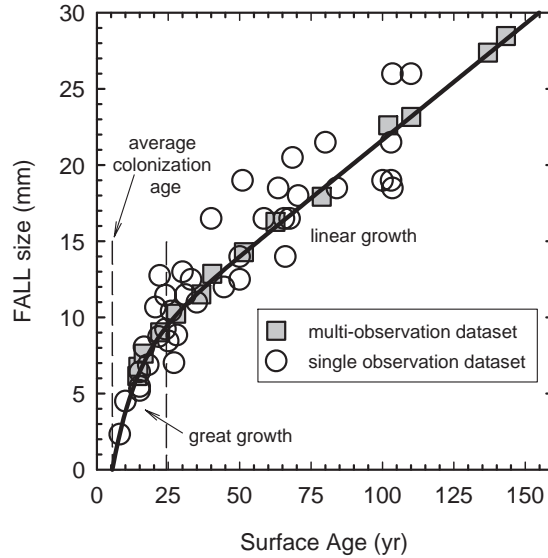


Figure 16. Best-fit solution for the four-parameter lichen-growth equation for New Zealand yellow rhizocarpons. Great-growth phase is between the dashed lines. Colonization time is shown by offset of the great-growth curve from the origin.

standard deviation of a single lichen size measurement in a FALL peak is $\sigma(D) \sim 2.4$ mm. The observed lichens with known substrate-exposure ages form a set of lichen sizes, D_i^{obs} , where $i = 1, \dots, n$, and the corresponding sizes predicted by equation 10 are designated D_i^{calc} . The best-fit parameters are determined by minimizing $\sum (D_i^{obs} - D_i^{calc})^2$, as summarized in Table 4.

The coseismic rockfall model assumes that the largest lichen on each rockfall block was the first to colonize the fresh substrate. Thus, it is important to consider the probability distribution of times needed for the first lichen to colonize. Colonization can be viewed as a Poisson process if the average rate of colonization is everywhere constant. This assumes that the average flux of spores across the study area remains constant in time and space, that all favorable surfaces have an equal probability of being colonized, and that the colonization events are independent and randomly distributed across all favorable surfaces. The distribution of first events for a Poisson process is described by the exponential distribution (equivalent to the gamma distribution with $\alpha = 0$; see Selby, 1970, p. 572; Press et al., 1992, p. 282),

$$p(\tau_c) = \frac{1}{\tau_0} e^{-\tau_c/\tau_0}, \quad (11)$$

where p is the probability density as a function of colonization time τ_c , and τ_0 is the mean colonization age. The mean and standard deviation are equal for this distribution: $\tau_0 = \mu(\tau_c) = \sigma(\tau_c)$. The example in Figure 17A uses $\tau_0 = 5.4$ yr, which is

equal to the estimate given in Figure 16. The colonization-time distribution (Figure 17A) can be transformed into a predicted FALL distribution at 150 yr (Fig. 17B) using the lichen growth curve given by equation 10, assuming colonization to be the only factor influencing the structure of the peak. The calculated standard deviation for the transformed distribution is $\sigma = 0.9$ mm. This example shows that block-to-block variations in colonization time can cause a maximum variation in FALL size of $\sim \pm 2.1$ mm (equal to $\pm 3\sigma$) around the FALL mean. This means that the colonization process alone produces variations in FALL sizes equal to an apparent age variation of $\sim \pm 18$ yr ($\sim \pm 3\sigma$).

About 20 to 30 yr may be needed for initial colonization of all blocks generated by a given New Zealand rockfall event (Fig. 17A). The resulting lichen-size distribution for rock surfaces younger than 30 yr will have a large-side bias because those lichens that will eventually make up the small-side part of the distribution have yet to become established. A partial solution to this sampling problem is to use equation 10 to transform all young lichens to a common age (Fig. 17A). The transformation equation is,

$$D(\tau_r) = D(\tau) + D_0 e^{-K\tau_0} (e^{-K\tau} - e^{-K\tau_r}) + C(\tau_r - \tau), \quad (12)$$

where τ is the known substrate-exposure age, τ_r is the reference age ($\tau_r = 150$ yr in Fig. 17B), $D(\tau)$ is the measured lichen size, and $D(\tau_r)$ is the predicted size at τ_r .

LICHEN DATING OF NEW ZEALAND ROCKFALL EVENTS

TABLE 3. CALIBRATION SITES AND DATA USED TO DEFINE GREAT-GROWTH AND UNIFORM GROWTH PHASES FOR *RHIZOCARPON* SUBGENUS *RHIZOCARPON* IN THE STUDY REGION ON THE BASIS OF FALL MEASUREMENTS

Calendric date of historical deposit (yr, A.D.)	Characteristics of lichenometry calibration site	FALL peak mean lichen size (mm)	Standard error of peak mean (mm)	Peak width (standard deviation, mm)	Peak size (count)
1983.21	Boulder bar deposited at the mouth of the Charwell River gorge during rainy El Niño year. Measured in 1997.38.	6.149	0.3140	1.88	36
1982.90	Construction of road on Puhī Peaks farm exposes fractured graywacke. Measured in 1997.41.	6.751	0.2566	1.41	30
1981	Construction of infiltration gallery leaves cobble piles on the floodplain of Charwell River. Measured in 1997.38.	7.619	0.4955	2.10	18
1975.20	Cobble and boulder bar deposited at the mouth of the Charwell River gorge at time of Cyclone Alison flood. Measured in 1997.38.	9.011	0.3660	2.23	37
1969.61	Boulders removed from field on terrace of the Charwell River. Measured in 1997.38.	10.24	0.2763	2.01	53
1957	Boulder and cobble bar deposited at the mouth of the Charwell River gorge. Measured in 1997.38.	12.85	0.3130	2.75	77
1955.45	Mass movement deposits near earthquake epicenter. Not witnessed, but local residents described coseismic landslides. Age of earthquake known to the day. Measured in 1992.	11.51	0.1230	0.615	25
1940.5	Wall near Flock Hill studied by Orwin (1970, 1971). Age estimate is time of construction date for this flood protection wall (± 0.5 yr). Measured in 1992.	14.28	0.1803	1.42	62
1929.46	Mass movement deposits near earthquake epicenter. Not witnessed, but photographs were taken after the earthquake of the Rough Creek landslides and the 60×10^6 m ³ Falling Mountain rock avalanche. Date of Arthur's Pass earthquake was 1929.22, but 1929.46 date of much larger Murchison earthquake is used in the calibration. Measured in 1992.	16.27	0.0408	0.809	393
1913.25	Outburst flood deposit of the Mueller Glacier. Eye witnesses date destruction by this flood to the day. Measured in 1992.	17.92	0.2051	4.02	384
1890	Outburst flood deposit of the Tasman Glacier. Not witnessed, but guides use the vegetation-free flood deposit as a new access route to the glacier. Age estimate is ± 0.5 yr. Measured in 1992.	22.61	0.1626	0.920	32
1881.93	Mass movement deposits near earthquake epicenter. Other control points used for an assumed age, which then was verified by a rockfall-abundance map that shows that greatest seismic shaking occurred near the epicenter of the earthquake, whose age is known to the day. Measured in 1992.	23.16	0.1205	2.07	295
1855.06	Mean lichen size from 20-site regional data set ($n = 3866$). Other control points used for an assumed age, which then was verified by a rockfall abundance map that shows that greatest seismic shaking occurred near the epicenter of the earthquake, whose age is known to the day. Measured in 1992.	27.38	0.0953	0.286	9
1848.79	Same as for the 27.38 mm FALL peak.	28.47	0.0696	0.400	33

Note: Peak means, standard errors, widths, and sizes are from decomposed density plots. The standard error for the peak mean is estimated as the peak width divided by the square root of the peak size. It approximates the uncertainty in the peak mean that would be observed in analysis of many replicate FALL distributions.

TABLE 4. CALIBRATION OF LICHEN GROWTH EQUATIONS

Description	A (mm)	B (= -C) (mm/yr)	τ_0 (yr)	D_0 (mm)	K (yr ⁻¹)
Four parameter equation using data in Table 3, and 40 single observation data; 54 calibration points, 1524 lichens, $\sigma(D) \approx 2.4$ mm.	310.183	-0.1525 (± 0.0030)	5.43 (± 2.2)	7.22 (± 0.33)	0.1219 (± 0.0353)
Two parameter equation using sites older than 1956 in Table 3; 8 calibration points, 1233 lichens, $\sigma(D) \approx 2.5$ mm.	307.289 (± 46.6)	-0.1510 (± 0.0244)	N.A.	N.A.	N.A.
Two parameter equation using sites older than 1956 in Tables 3 and 4; 19 calibration points, 3438 lichens.	311.889	-0.1535	N.A.	N.A.	N.A.

Note: Uncertainties given at ± 1 standard error. N.A. = not available.

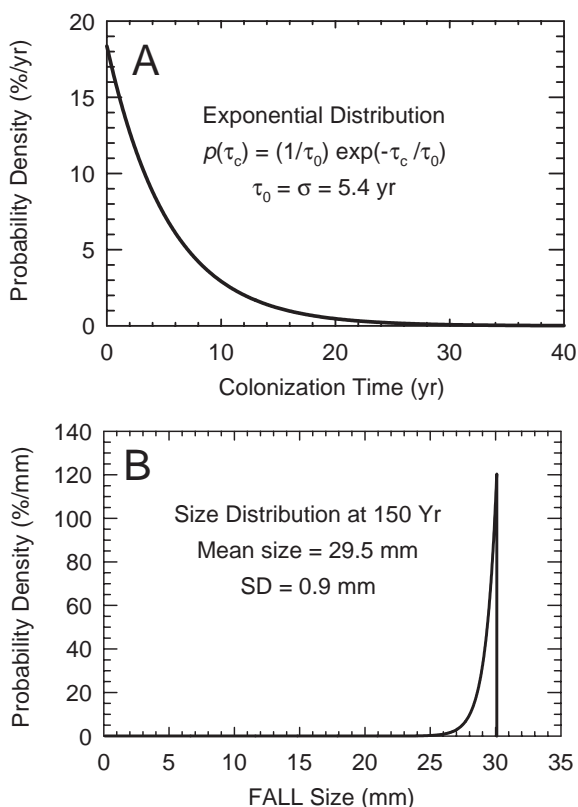


Figure 17. The distribution for lichen colonization time as predicted by the first arrival times for a Poisson process. (A) Predicted distribution for arrival times of the first lichen. (B) Distribution of lichen sizes after 150 yr, assuming that the only variation is in colonization time shown in Figure 17A.

Equation 10 can be simplified if lichen growth has reached the uniform-growth phase. First, we need to introduce ζ , which indicates the degree of completion of the great-growth phase as represented by the first term in equation 10,

$$\zeta = 1 - e^{-K(\tau - \tau_0)} \quad (13)$$

With infinite time, ζ will approach 1.0 asymptotically, which means that the first term in equation 10 has gone to 0. Using equation 13 and solving for τ as a function of ζ gives

$$\tau(\zeta) = \tau_0 - \frac{\ln(1 - \zeta)}{K} \quad (14)$$

We define great growth to correspond to the amount of time needed to complete 90% of the excess growth, D_0 , produced by great growth. Lichen size at the end of great growth is

$$D(\zeta = 0.90) = 0.9D_0 - \frac{C \ln(0.1)}{K} \quad (15)$$

For Figure 16, $\tau(90\%) = 24$ yr and $D(\zeta = 0.90) = 9.4$ mm. At this point, there is only 10% excess

growth that will occur, equal to another 0.7 mm increase in lichen size.

For the uniform growth phase, equation 10 simplifies to

$$D = (D_0 - C\tau_0) + C\tau \quad (16)$$

$$\tau = \left(\tau_0 - \frac{D_0}{C} \right) + \left(\frac{1}{C} \right) D \quad (17)$$

For field applications, we prefer to estimate the time of substrate-exposure in calendar years. The year when the surface of the rock-fall block was first exposed is defined by t and the year when the lichen was measured is defined by t_p . Equations 16 and 17 can be converted by substituting $t_p - t$ for τ .

$$D = \left[D_0 + C(t_p - \tau_0) \right] - Ct \quad (18)$$

$$t = \left[\frac{D_0}{C} + (t_p - \tau_0) \right] - \left(\frac{1}{C} \right) D \quad (19)$$

Equation 19 sets the stage for a simple calibration procedure.

CALIBRATION OF LICHEN GROWTH

Equation 10 uses great-growth and uniform-growth data sets to estimate four lichen growth parameters. Calibration based only on uniform-growth data sets, together with a simplified version of equation 19, uses the widely available linear regression method

$$D = A + Bt, \quad (20)$$

where D is the dependent variable and t the independent variable. A and B are fit parameters that relate to equations 18 and 19 according to $A = D_0 + C(t_p - \tau_0)$ and $B = -C$. Use of equation 20 requires that the peak means are larger than great-growth sizes, which for New Zealand is $D > 9.4$ mm.

The markedly different calibration plots for *Rhizocarpon* section *Alpicola* from the Otira Valley site in the Southern Alps, and *Lecidea atrobrunnea* in the Sierra Nevada of California illustrate how the linear regression method can be used to evaluate duration of lichen colonization time, and magnitude and rate of great growth (Fig. 18). Projection of the slow linear growth rate line for *R. Alpicola* intersects the time axis at A.D. 2027. A 1968 control point constrains the great-growth segment of the growth curve and indicates a colonization time of about 20 yr (four times longer than other yellow rhizocarpons). The uniform growth-rate line for *L. atrobrunnea* intersects the time axis at A.D. 1941, indicating a colonization time of >50 yr. The amount of great growth for *L. atrobrunnea* apparently is only half of that for *R. Alpicola*. Field studies of lichens on young substrates confirm that *L. atrobrunnea* has a long colonization time, short great-growth phase, and rapid uniform growth compared to *R. Alpicola*.

Precise calibration of lichen growth is possible in the Southern Alps because of (1) digital-caliper lichen-size measurements, (2) large data sets, (3) substrate-exposure dates for landslide and flood deposits that are known to the year or day, and (4) minimal between-site variation of lichen growth rates. Ideally, all FALL measurements used in calibration equation 20 should be made in the same year. FALL sizes measured in different years can be normalized, but only after an initial uniform growth rate has been estimated. For example, measurements of New Zealand yellow rhizocarpons made 6 yr apart would require a correction of 0.9 mm ($6.0 \text{ yr} \times 0.15 \text{ mm/yr} = 0.90 \text{ mm}$).

FALL measurements on deposits of known age provided eight control points to calibrate the uniform phase growth rate for yellow rhizocar-

pons (sites with dates older than 1956 in Table 3). These include the Flock Hill wall, two glacier-outburst flood deposits, three landslide deposits, and two points where FALL peaks can be correlated to a regional rockfall event caused by a known earthquake. One of the landslide sites was at Rough Creek (Fig. 11) where coseismic rockfalls were photographed in 1929. Two 1929 earthquakes occurred only 3 months apart at two widely separated epicenters (Table 2). These were the Arthur's Pass event: $M_s \sim 7.1$, depth < 15 km, right-lateral surface displacement; and the Murchison event: $M_s \sim 7.8$, depth < 20 km, reverse-oblique surface displacement (Speight, 1933; Dowdrick and Smith, 1990; Cowan, 1994).

A map of rockfall abundance based on sizes of best-fit FALL peaks (Fig. 19) provides additional confirmation for the 1929 date for the 16 mm FALL peak at the Rough Creek site. Response to seismic shaking associated with the Arthur's Pass earthquake appears to have been particularly intense near the epicenter. The Murchison earthquake caused more widespread and stronger seismic shaking. The climate is too wet for yellow rhizocarpons near the Murchison epicenter, so the peak-size map is incomplete near the epicenter.

Peak-size maps were used to confirm assignments of earthquake dates to specific FALL peaks for two calibration points. Rockfall abundance for the 28.47 mm peak was greatest near the epicenter of the 1848 Marlborough earthquake (Fig. 1, Table 2), but decreased to minimal values 150 km to the southwest. In marked contrast, the great 1855 West Wairarapa earthquake (27.38 mm peak) caused large rockfalls more than 500 km from its epicenter in the southern part of the North Island.

The Figure 20A calibration was determined by the linear-regression method. Weighting of the data was accomplished in the same way as for Figure 16, by generating for each FALL peak a Gaussian-distributed set of FALL sizes with a mean, standard deviation, and count equal to the mean, width, and count of the peak. The number of calibration points $N = 9$, whereas the number of data points $n = 1524$. The best-fit equation is

$$D = 307.289 - 0.1510t, \quad (21)$$

which is relative to an observation year of A.D. 1992. Uniform-phase growth is clearly linear at 15.1 mm per century. Substrates exposed at A.D. 0 would have a FALL mean of 307 mm in A.D. 1992, assuming that the lichens were still alive. (Note that A.D. 0 is not formally recognized on the calendar scale, but it would be equivalent to 1 B.C. given that this is the calendar year that preceded A.D. 1). The heavy gray curve shows the nonlinear curve of Figure 16 for comparison.

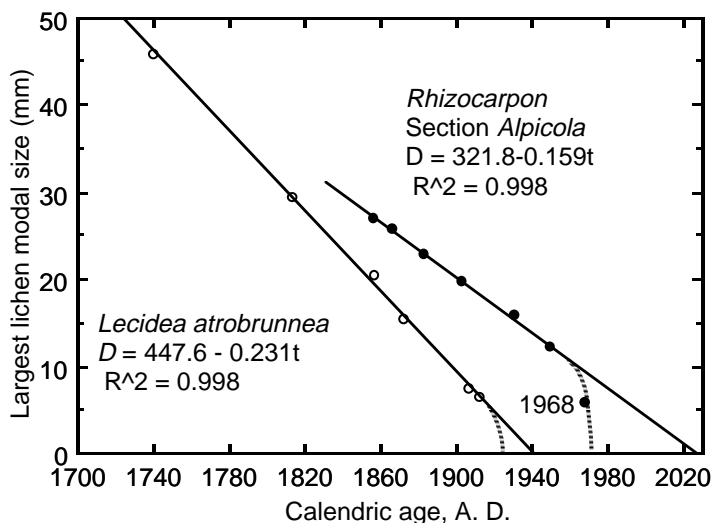


Figure 18. Comparison of growth rates for *Rhizocarpon section alpicola* at the Otira Valley site in the Southern Alps of New Zealand, and *Lecideia atrobrunnea* from the Sierra Nevada of California, using linear regression equation 20. Intersection of uniform phase regression lines with the X-axis constrains the maximum substrate-exposure date. Patterned lines show likely great-growth curves and substrate-exposure dates. Data sets are normalized to a 1992 measurement year.

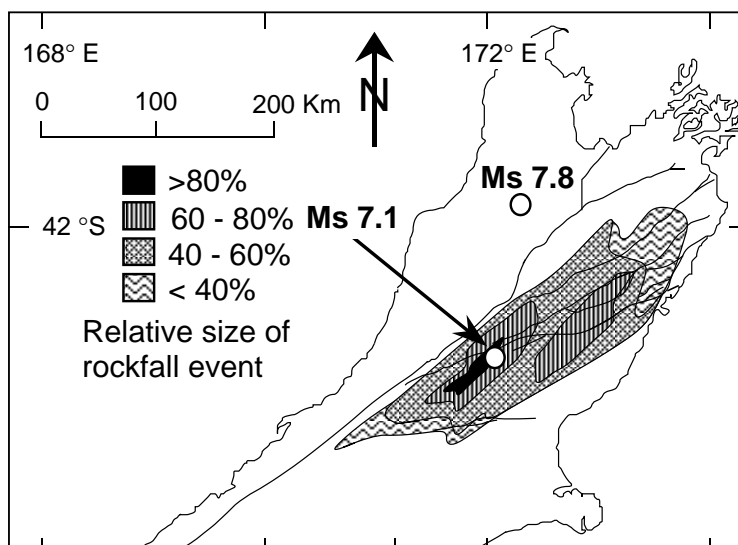


Figure 19. Peak-size map for the 16 mm regional rockfall event at 53 lichenometry sites showing the combined effects of seismic shaking induced by the 1929 M_s magnitude 7.1 and 7.8 earthquakes (Table 2). Contours show the percentage of the 16 mm modeled peak size relative to all FALL measurements between 13 and 19 mm.

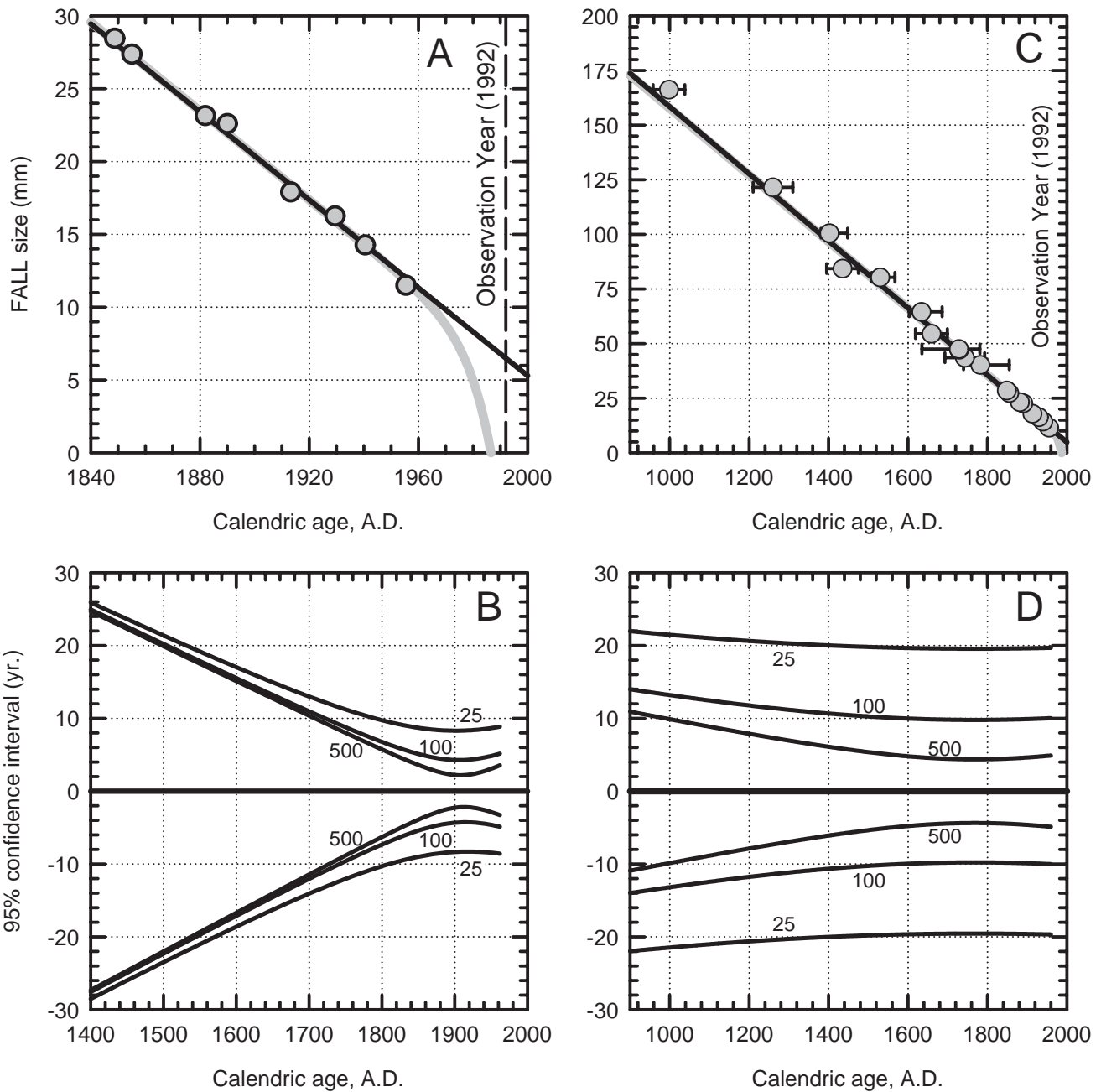


Figure 20. Calibration results illustrating the importance of data set size and age range in calibrating the lichen growth equation. Data are from Tables 3 and 5 and were restricted to sites older than 1956 to ensure that the calibration was entirely within the uniform-growth phase. Note that the heavy gray line in parts A and C shows, for comparison, the four-parameter growth curve of Figure 16. (A) Calibration using eight historic calibration points spanning 150 yr. Regression results were calculated using D as the dependent variable and t as the independent variable. The plot symbols are larger than the two standard error uncertainties for age and FALL size. (B) The 95% confidence interval for an estimated lichenometry age using the calibration in A. The contoured values 25, 100, and 500 refer to the number of FALL measurements used to estimate the FALL peak to be dated. (C) Calibration using a combined data set of 19 calibration points, both historic and prehistoric, spanning 1000 yr. Regression results were calculated with t as the dependent variable and D as the independent variable. Error bars show the one-standard-error uncertainties. (D) The 95% confidence interval for an estimated lichenometry age. The contoured values 25, 100, and 500 refer to the number of FALL measurements used to estimate the FALL peak to be dated.

Preliminary Long-Term Calibration

Prehistoric (before A.D. 1840) FALL peaks that can be correlated with reasonably well-dated paleoseismic events provide useful insight in two ways. They can be used to validate equation 21, and to illustrate how a change in the range of ages for calibration control points affects the uncertainties of lichenometry age estimates (Fig. 20B). The 11 prehistoric calibration points include nine radiocarbon age estimates and two forest disturbance events (Table 5).

Cowan and McGlone (1991) concluded that episodes of silt deposition in Raupo swamp (Fig. 1) were related to paleoseismic disruption of hillslopes that drained into the swamp. Pollen in the peat above each silt layer records a transition from disturbance-type plants, such as the shrub *Discaria toumatou*, to plants indicative of stable hillslopes. Calibrated radiocarbon ages were used to calculate the peat-accumulation rate in order to date the coseismic silt layers. Age estimates for five silt layers, and older landslide-buried trees in the banks of the nearby Hope River range from A.D. 1260 to 1782; each most probable age (without individual uncertainty ranges) is within ± 30 yr of a lichenometry estimate for the age of a strong regional rockfall

event. The Table 5 FALL peaks are shown in Figure 7. Radiocarbon age estimates of trees buried by the Clyde, Acheron, and Craigieburn rock avalanches (Burrows, 1975; Whitehouse, 1981; Whitehouse, 1983), together with FALL measurements on the rock avalanches provide three calibration points.

This regression calculation is different from the previous one because the uncertainties associated with time are greater than those associated with FALL size. As such, the regression equation must be recast so that t is the dependent variable, and D is the independent variable. Weighting in this case was done by generating for each FALL peak a bivariate Gaussian-distributed set of FALL sizes and ages equal in number to the count of each peak. FALL size was varied to mimic the mean and width of the associated FALL peak. Age was varied according to the means and uncertainties cited in Table 5. Average uncertainties were used for those ages with unequal uncertainties in order to ensure symmetric distributions as required for the regression method. A peak width of 2.5 mm was assumed for all of the FALL peaks in Table 5.

The combined historic and prehistoric calibration points (Tables 3 and 5) for sites older than 1956, define lichen growth as

$$D = 311.889 - 0.1535t \quad (22)$$

Equations 21 and 22 are nearly identical, which indicates that the constant rate associated with the uniform-growth phase appears to extend back for 1000 yr.

We have some reservations about the long-term calibration because all the age estimates for the prehistoric control points have potential problems. Three of the radiocarbon ages may be 30 to 100 yr older than the landslides they date. Except for the Acheron sample, chunks of wood, instead of only the outermost tree rings, were dated. Dates for the Raupo Swamp silt layers assume that peat-accumulation rates have been constant. The forest disturbance events are not dated to the year; rimu (*Dacrydium cupressinum*) does not cross date (the dendrochronology method used to make sure that annual growth rings are not missing or duplicated). In light of this, simple ring counts were made to estimate germination ages or time of damage. We prefer to use equation 21 for events back to A.D. 1848 and equation 22 for events older than A.D. 1848.

TABLE 5. DATA FROM PREHISTORIC SITES THAT WERE USED FOR A LONG-TERM CALIBRATION OF THE GROWTH OF *RHIZOCARPON* SUBGENUS *RHIZOCARPON*

Calendric age estimate (yr, A.D.)	Peak mean lichen size (mm)	Peak size (count)	Dating method used to estimate calendric age Lichenometry site characteristics
1782 +73 -42	40.25	560	Radiocarbon age for coseismic silt layers in a peat bog along the Hope River segment of the Hope fault (Cowan and McGlone, 1991), compared with lichenometry age for a regional rockfall event.
1743 ± 50	43.53	410	Major disturbance event in a rimu forest described by Conere (1992) and modeled by Bull (1996a).
1729 ± 5	47.20	250	Tree-ring counts on 25 podocarps on fault scarp near Haupiri (Andrew Wells, Lincoln University, New Zealand, 1997, personal commun.), compared with lichenometry age for a regional rockfall event.
1728 +53 -93	47.50	270	Radiocarbon age for coseismic silt layers in a peat bog along the Hope River segment of the Hope fault (H. Cowan, 1994, personal commun.), compared with lichenometry age for a regional rockfall event.
1659 ± 40	54.50	300	Radiocarbon age for wood buried by the Clyde rock avalanche (Whitehouse, 1983).
1634 +52 -31	64.50	150	Radiocarbon age for coseismic silt layers in a peat bog along the Hope River segment of the Hope fault (Cowan and McGlone, 1991), compared with lichenometry age for a regional rockfall event.
1530 +37 -21	80.30	130	Radiocarbon age for coseismic silt layers in a peat bog along the Hope River segment of the Hope fault (Cowan and McGlone, 1991), compared with lichenometry age for a regional rockfall event.
1435 ± 40	84.27	140	Radiocarbon age for twigs buried by the Acheron rock avalanche (Burrows, 1975).
1402 +46 -21	100.50	23	Radiocarbon age for coseismic silt layers in a peat bog along the Hope River segment of the Hope fault (Cowan and McGlone, 1991), compared with lichenometry age for a regional rockfall event.
1260 ± 50	121.50	16	Radiocarbon age of wood in the Hope River Bridge landslide, dated by the old solid carbon counting method (Cowan and McGlone, 1991).
998 ± 40	166.26	6	Radiocarbon age for wood for part of the Craigieburn rock avalanche (Whitehouse, 1981). Lichen data from Craigieburn rock avalanche and nearby sites. Radiocarbon ages are consistent with weathering-rind dating of 8 synchronous rock avalanches studied by Griffiths (1983) and modeled by Bull (1996a).

Note: Measurements were made in 1992, or normalized to 1992. Age uncertainties are ± 1 standard error.

LICHENOMETRY AGE ESTIMATES

Our coseismic rockfall model allows a robust appraisal of lichenometry as a dating method. This section addresses several key questions: How is the precision of lichenometry age estimates affected by the sizes and age range of the calibration control points? What are the advantages of having many independent age determinations for an event, instead of only one age estimate? Which field and data analysis methods should be used to describe and date regional rockfall events that are closely spaced in time? What is the accuracy of the lichenometric approach to surface-exposure dating in New Zealand?

Uncertainties

Figures 20B and 20D show the 95% confidence intervals for the two calibrations. The methods used for calculating these intervals are discussed in Mandel (1964, p. 278–281) and Draper and Smith (1966, p. 21–24). The appropriate procedure to be used is influenced by the different ways that the calibrations were done, with D as the dependent variable in Figure 20A and t as the dependent variable in Figure 20C.

Equation 12.25 from Mandel (1964) was used to calculate the 95% intervals for Figure 20B. For this case, his variable N is the total number of lichens (1233) in the eight calibration points. There are eight independent calibration points and two fit parameters, which means that the degrees of freedom are six. The Student t distribution was used to estimate confidence intervals from the standard error determined for the predicted time, t .

The calculation for the 95% intervals in Figure 20D follows that of equation 1.4.7 from Draper and Smith (1966). Their variable s is estimated from the residuals from the regression calculation (i.e., the misfit between observed and calculated t). Their variable $n = 3438$ is the total number of lichens measured in the 19 calibration points. We increased the standard error of t given by their equation 1.4.7 by the amount

$$B\sigma(D)\sqrt{m},$$

where B is the slope of the calibration line, $\sigma(D)$ is the standard deviation of a single size measurement for lichens in a FALL peak, and m is the number of lichen measurements in the unknown FALL peak to be dated. This modification accounts for the influence that the number of lichens in the unknown FALL peak has on the uncertainty of the estimate lichenometry age. $\sigma(D)$ was estimated to be ~ 2.5 mm. For Figure 20D, there are 19 independent calibration points and two fit parameters, which means that the de-

grees of freedom are 17. Once again, the Student t distribution was used to estimate confidence intervals from the standard error determined for the predicted time, t .

The estimated confidence intervals include the uncertainties associated with the calibration line and the uncertainties of the estimated mean for the FALL peak to be dated. For Figure 20B, the confidence intervals expand greatly for extrapolations beyond the A.D. 1848 to 1955 calibration range. Within the calibration range, it is possible to estimate lichen ages to better than ± 10 yr for FALL peaks with more than 25 measurements. By comparison, the extended calibration shown in Figure 20 (C and D) has a much tighter uncertainty. FALL peaks with 100 to 500 measurements can be dated to a precision of better than ± 15 yr back to ages of A.D. 1000 and older. Figure 20 illustrates the important role that the calibration curve plays in influencing the uncertainty for an estimated lichenometry age. The uncertainty of an age estimate for a FALL peak can be improved by increasing the number of measured lichens, but beyond about 100 to 200 lichen-size measurements, the uncertainty becomes limited by the quality of our calibration.

Resolution

We examined the resolution of the coseismic rockfall model, initially using a large FALL data set combined from four sites that are only 2 to 4 km from the Conway segment of the Hope fault (Fig. 21). The 28.70 mm peak probably records the oldest historical earthquake for this study area, one that had an epicenter approximately 110 km away (Table 2). Applying equation 21 or 22, this peak dates to about 1845. The 29.43 and 30.36 mm peaks predate the first substantial influx of European colonists into New Zealand in 1840. Two events in the 29–31 mm range are recorded at many sites; mean peak sizes are 29.5 and 30.4 mm at 47 and 46 sites, respectively.

Decomposition of the density plot of estimated ages for the combined 47 site data set (Fig. 22) into its component Gaussians reveals a third and smaller peak that is not apparent at the Hope fault sites (Fig. 21). Estimated calendric ages for the three presumed prehistorical earthquakes are about A.D. 1840, 1836, and 1833. Are these closely spaced peaks real, or they are merely noise?

The hypothesis of three regional coseismic rockfall events during a 7 yr time span between A.D. 1833 and 1840 can be tested with peak-size maps to locate the epicentral regions for the three earthquakes. The peak-size pattern for the 30 mm event (Fig. 23A) is suggestive of a composite pattern of seismic shaking associated with the two older earthquakes. The A.D. 1833 event occurred along the Conway segment of

the Hope fault, as is suggested by the Figure 23A peak-size map, and confirmed by FALL measurements on disrupted outcrops within 4 km of the fault trace (Bull, 1997). The other event appears to be smaller and occurred in A.D. 1836 near the western edge of the study area. The simple pattern of peak size associated with the 29 mm FALL event (Fig. 23B) clearly suggests seismic shaking associated with a single large A.D. 1840 earthquake in the central part of the study area, perhaps along the Awatere fault. Peak sizes for the A.D. 1840 event are anomalously low near the Conway segment of the Hope fault, most likely because the A.D. 1833 earthquake had already dislodged most of the unstable blocks. The internal consistency of the two peak-size maps and the three FALL peaks of Figure 22 supports the hypothesis of three earthquakes in 7 yr.

Lichenometry age estimates can be tested using independent historical or tree-ring dated events known to the year. Comparison of historical earthquake dates with lichenometry age estimates for Figure 15B modeled peaks suggests a mean difference of 3 ± 4 yr. This departure is about the same as noted for accuracy of lichenometry in the Sierra Nevada of California, 2 ± 4 yr (Bull, 1996b).

APPLICATIONS

The FALL approach to surface-exposure dating can be used in other geomorphic studies to determine the frequency of hillslope, fluvial, coastal, glacial, and periglacial processes. Closely spaced geomorphic events can be dated with much better precision than by radiocarbon dating. Examples include rockfall accumulation rates (Luckman and Fiske, 1995), frequency of debris flows (Rapp, 1981; Innes, 1983), and landslide-hazard evaluation (Bull, et al., 1994). FALL measurements can decipher the composite nature of young glacial moraines, stream-terrace treads, and beach ridges. Glacial moraines that appear to have been emplaced at one time typically have several distinct lichen-size peaks (Proctor, 1983; Bull et al., 1995, Fig. 8).

Reliability of lichenometric dating of geomorphic processes is best where substrate-exposure time is the same for all blocks and is poor where many blocks have inherited lichens. Blocks carried on the surface of a glacier may have lichens that predate their deposition in a moraine. In contrast, large rock avalanches and block slides generally exhume deep-seated joint blocks. Furthermore, there is minimal chance of survival of inherited lichens if the landslide detritus is mixed during rapid transport over long distances. Well-mixed rock avalanches and block slides will typically result in a single FALL peak with virtually no inherited lichens (Bull et al., 1994, Fig. 5).

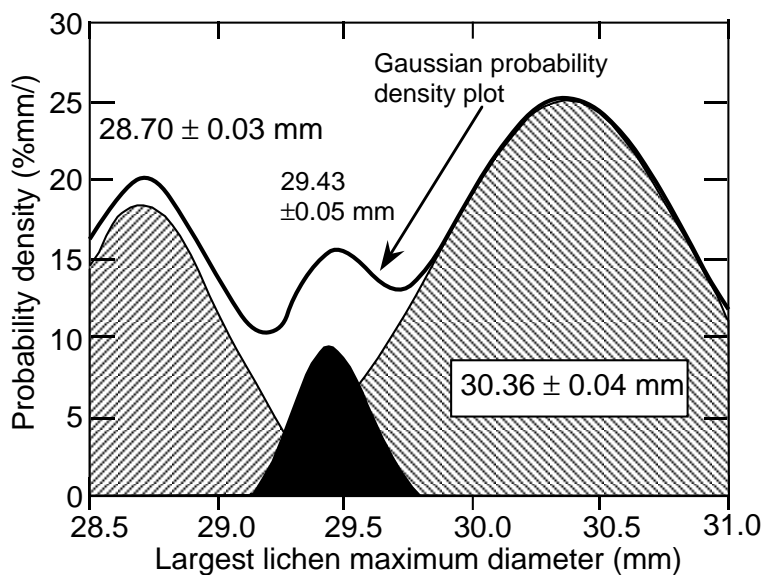


Figure 21. Three principal FALL peaks modeled for a probability density plot composed of data combined from the Stone Jug and Goat Hills sites. Gaussian kernel size is 0.1 mm; $n = 297$.

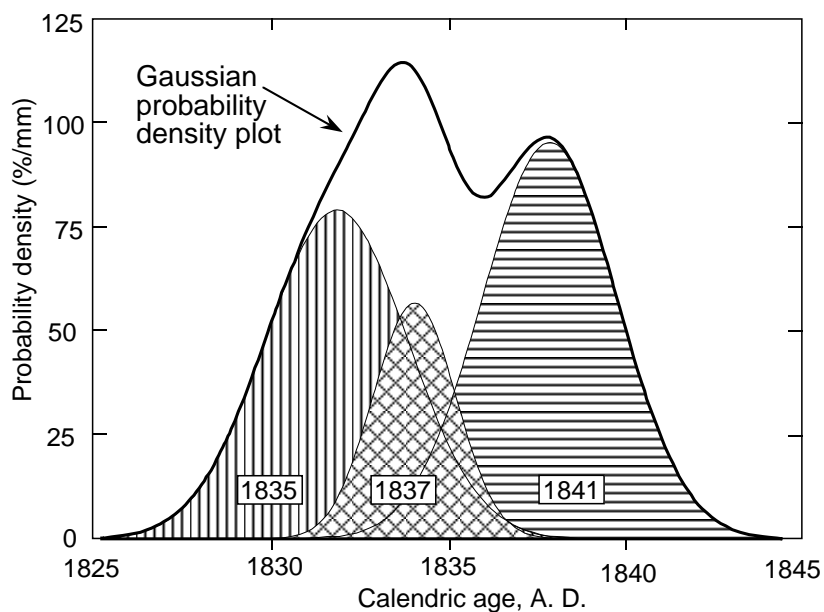


Figure 22. Decomposition of a density plot of times of regional rockfall events at 47 lichenometry sites suggests that three coseismic events occurred in 6 yr. Gaussian kernel size is 1.0 yr.

Small, shallow mass movements generally contain blocks with inherited lichens; their FALL data sets tend to be polymodal. Half the blocks on debris-flow levees may have inherited lichens if blocks from source hillslopes are shoved downslope with minimal mixing, or are incorporated from nearby older debris-flow deposits. Like most glacial moraines, the FALL distributions for such debris flows commonly are highly skewed toward larger FALL sizes, making it difficult to distinguish the peak that records the event date from older and younger peaks.

Event magnitude is revealed by the areal extent of lichens belonging to a specific FALL distribution. Examples include episodes of slush-avalanche deposition on a fan (Bull et al., 1995), trimlines on bedrock that record closely spaced advances of a valley glacier (Mahaney, 1987), and bouldery flood deposits.

Lichenometry adds new dimensions to studies of prehistoric earthquakes. Dating of earthquakes has been limited mainly to digging trenches across fault scarps and dating the times of stratigraphic disturbance caused by surface ruptures (e.g., McCalpin, 1996, p. 47–75). Access to fault scarps is not needed in the lichenometric approach to paleoseismology, and, because of this, recent earthquakes associated with blind thrust faults and offshore subduction zones can be studied. For example, Bull (1996a, Fig. 13) used peak-size maps to describe patterns of seismic shaking associated with three Alpine fault earthquakes, even though none of his lichenometry sites were within 20 km of the fault trace. Systematic regional trends depicted by peak-size maps (see Figs. 19 and 23) provide the same level of information as Modified Mercalli Intensity maps (Cowan, 1991; Downs, 1995).

Surface-exposure dating methods avoid two inherent problems with stratigraphically based isotopic dating. Dated organic matter either predates or postdates the time of an earthquake, and isotopic production rates may vary, resulting in multiple apparent ages for a single young sample (Stuiver and Reimer, 1993). Thus, lichenometry can be more precise than radiocarbon dating, and may also be more reliable and credible than stratigraphic radiocarbon dating of earthquakes. Periods of nondeposition are difficult to recognize at stratigraphic paleoseismic sites (Cowan and McGlone, 1991) but are crucial because earthquake(s) that occur during a depositional hiatus may not be recognized. Omission of one or more events can seriously bias an earthquake-recurrence evaluation (Bull, 1996b).

The coseismic-rockfall lichenometry approach to paleoseismology is best used in mountain ranges characterized by lichens growing on smooth, planar rock surfaces, historical earthquakes with Mw magnitudes of 6 to >8, and un-

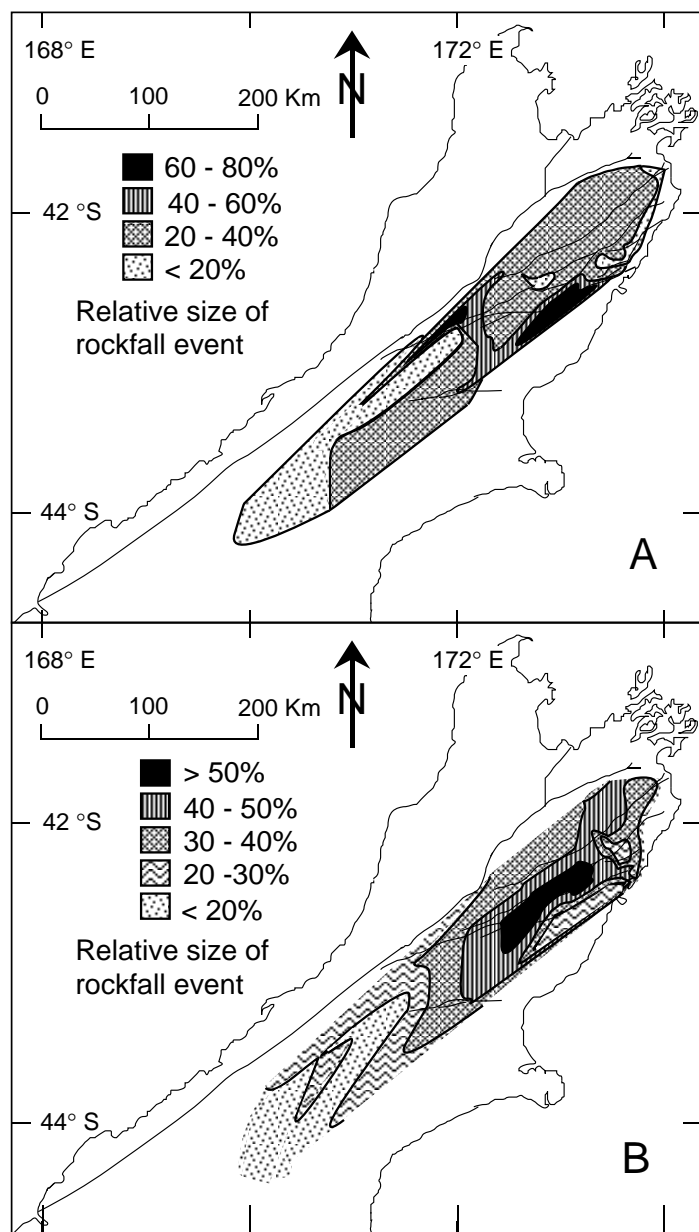


Figure 23. Peak-size maps for three regional events. Contours show the percentage of the 29 or 30 mm modeled peak size relative to all FALL measurements between 27 and 33 mm. (A) Map for the 30 mm FALL event indicates two areas of highest seismic shaking on the edges of the study region. (B) Map for the 29 mm FALL event shows one area of seismic shaking in the center of the study region.

stable outcrops as indicated by the presence of talus and debris slopes. Lichenometry has been used to estimate earthquake recurrence intervals, as well as the time that has elapsed since the most recent earthquake (Bull, 1996a). The local fault responsible for a prehistorical earthquake can be identified by using fractured bedrock sites that respond only to intense, local shaking (Bull, 1997).

Our calibration method can also be used in nonseismic regions by measurement of FALL sizes on dated landslide, flood, volcanic, and glacial deposits; and on highway, railroad, and trail cuts, or dam embankments that mimic rocky hillslopes (Bull et al., 1995). Synchronously exposed rock surfaces in nonseismic mountain ranges can also be used to assess the influence of

regional climatic gradients on lichen growth rates. Examples of potentially useful geomorphic surfaces include extensive historical flood gravels and lava flows, and regional episodes of avalanche and debris-flow activity triggered by major storms. Outcrops and detritus exposed by construction of transportation and utility routes across mountain ranges also may be used to determine if a single calibration can be used at many sites.

CONCLUSIONS

Lichenometry has several advantages and limitations. The cost per age estimate is small, and ages are obtained quickly where lichen growth rates are calibrated. Slow- and fast-growing lichens are common on rock substrates in much of the world, and use of several genera allows validation of age estimates (Winchester, 1984; Bull, 1996b). Limitations include the experience required to select suitable study sites and the time needed to collect large data sets. Lichenometric dating generally is limited to the past 500 yr. Taxonomic identification of hundreds of measured lichens is not practical, even at the section level. Furthermore, few lichenometrists have the botanical skills needed to detect subtle differences at the species level.

The potential of lichenometry to date geomorphic events of the past 500 yr precisely is best achieved by:

1. Making FALL measurements with digital calipers in order to increase precision and reduce bias.
2. Measuring the long axes of elliptical thalli, which record optimal lichen growth.
3. Measuring only exposed lichens to minimize microclimatic effects on lichen growth rates.
4. Measuring large FALL data sets and using peak-fitting methods to estimate the mean, area, and width of significant peaks.
5. Calibrating lichen growth rates with sites dated to the year or day. Examples include tree-ring analyses of a forest killed by a prehistorical landslide or volcanic eruption (Smiley, 1953, Yamaguchi, 1985; Bull et al., 1994) or historical substrate-exposure events.
6. Determining the spatial validity for calibration of lichen growth rates by comparing FALL distributions on substrates formed at the same time at different altitudes and climatic settings, and on different rock types.

Our study of synchronous earthquake-generated rockfalls helps to remove a persistent cloud of uncertainty that has hovered over lichenometry. Calibration of lichen growth is not necessary at every study site because factors such as substrate lithology and smoothness, mean annual precipitation and temperature, and length of growing season do

not noticeably affect colonization times or growth rates of many species of *Rhizocarpon* subgenus *Rhizocarpon* growing at 90 sites in the Southern Alps of New Zealand. However, microclimate does influence growth rates; yellow rhizocarpons are larger where partly shaded and sheltered. The influence of local microclimate can be reduced by only measuring those lichens with a similar degree of exposure to sun and wind.

Regionally constant lichen growth rates greatly simplify calibration procedures. Calibration data sets with both great-growth phase and uniform phase control points can use equation 10 to describe the average colonization time, the nonlinear component of growth during the great-growth phase, lichen size at the end of the great-growth phase, and the constant growth rate during the uniform-growth phase. Calibration data sets consisting only of uniform-growth phase control points can use equation 21 to define lichen age as the sum of all three phases of lichen growth, and to make general estimates of colonization time and amount of great growth. Reporting of ages in calendric years eliminates the need for a master reference year, such as the A.D. 1950 radiocarbon dating reference year. Uniform-phase growth rate does not change with the year in which FALL measurements were made, but the constant A in equation 20 that describes growth since the year B.C. 1 (= A.D. 0) is a function of measurement year.

Lichenometry does not match the dating resolution of dendrochronology, but it can be much more precise and accurate than radiocarbon dating, especially for the past 300 yr. Like dendrochronology, lichenometry is based on an empirical relation between age and a biological phenomenon. Complex botanical dating methods are not easily summarized by laws of physics, such as those describing the decay of radioactive isotopes. Nevertheless, lichenometry has excellent potential as a surface-exposure dating method for disciplines as diverse as archaeology, geomorphology, and paleoseismology.

Our approach improves the resolution and precision of lichenometry. Excellent resolution is suggested by the consistent ability to separate pairs of regional rockfall events only 6 yr apart. Events only 2 to 4 yr apart may be dated, and the epicentral regions of the earthquakes that caused them can be located, when one takes the additional steps of preparation of FALL peak-size maps and making FALL measurements on outcrops near suspect fault zones. We conclude that the 95% confidence level uncertainties for New Zealand lichenometry ages of the past 600 yr, using peaks with >100 measurements, can be reduced to better than ± 10 yr. The level of precision achieved depends on proximity of the peak being dated to the age range of the calibration points, but

can be improved where multiple independent lichenometry age estimates are available, or when the age range of calibration sites is increased.

ACKNOWLEDGMENTS

This work was supported by the National Geographic Society, the U. S. National Science Foundation, and the Department of Geological Sciences, University of Canterbury, New Zealand. We are especially grateful to the many New Zealand farmers and the university and governmental scientists who generously assisted with advice, equipment, and permissions. Trevor Chinn, Hugh Cowan, Fanchen Kong, Elsa McGilvary, Mauri McSaveney, Tom Moutoux, Elise Pendall, Jarg Pettinga, William Phillips, Nancy Sprague, Kirk Vincent, and Mark Yetton provided valuable discussions during this 7-year project, and measured some of the lichens. Fanchen Kong provided probability density plots of FALL measurements and modeled component distributions that were used to prepare peak-size maps. Review comments by Bill Locke, William McCoy, and John Innes provided important insights as to how to improve the organization and logic of this paper.

REFERENCES CITED

- Aitken, J. J., and Lowry, M. A., 1995, More earthquakes explained: New Zealand Institute of Geological and Nuclear Sciences Information Series 35, 30 p.
- Andrews, J. T., Davis, P. T., and Wright, C., 1976, Little Ice Age permanent snowcover in the eastern Canadian Arctic: *Geografiska Annaler*, v. 58A, p. 71–81.
- Benedict, J. B., 1967, Recent glacial history of an alpine area in the Colorado Front Range, U.S.A. 1. Establishing a lichen growth curve: *Journal of Glaciology*, v. 6, p. 817–832.
- Benedict, J. B., 1988, Techniques in lichenometry—Identifying the yellow rhizocarpons: *Arctic and Alpine Research*, v. 20, p. 285–291.
- Benedict, J. B., 1990, Lichen mortality due to late-lying snow: Results of a transplant study: *Arctic and Alpine Research*, v. 22, p. 81–89.
- Benedict, J. B., 1993, A 2000-year lichen-snowkill chronology for the Colorado Front Range, USA: *The Holocene*, v. 3, p. 27–33.
- Beschel, R. E., 1950, Flechten aus Altersmaastab rezenter, moränen (Lichens as a yardstick of age of late-glacial moraines): *Zeitschrift für Gletscherkunde und Glazialgeologie*, v. 1, p. 152–161.
- Beschel, R. E., 1957, A project to use lichens as indicators of climate and time: *Arctic*, v. 10, p. 60.
- Beschel, R. E., 1959, Lichenometrical studies in West Greenland: *Arctic*, v. 11, p. 254.
- Beschel, R. E., 1961, Dating rock surfaces by lichen growth and its application to the glaciology and physiography (Lichenometry), in Raasch, G. O., ed., *Geology of the Arctic*: Toronto, University of Toronto Press, p. 1044–1062.
- Beschel, R. E., 1963, Geobotanical studies on Axel Heiberg Island in 1962, in Müller, F., ed., *Axel Heiberg Island Preliminary Report 1961–62*: Montreal, Canada, McGill University, p. 199–215.
- Bevington, P. R., 1969, Data reduction and error analysis for the physical sciences: New York, McGraw-Hill, 336 p.
- Bickerton, R. W. and Matthews, J. A., 1992, On the age of lichenometric dates—An assessment based on the 'Little Ice Age' moraine sequence of Nigardsbreen, southern Norway: *The Holocene*, v. 2, p. 227–237.
- Birkeland, P. W., 1981, Soil data and the shape of the lichen growth-rate curve for the Mount Cook area: *New Zealand Journal of Geology and Geophysics*, v. 23, p. 443–445.
- Brandon, M. T., 1992, Decomposition of fission track grain age distributions: *American Journal of Science*, v. 292, p. 535–564.
- Brandon, M. T., 1996, Probability density plots for fission-track grain-age samples: *Radiation Measurements*, v. 26, p. 663–676.
- Bull, W. B., 1991a, New Ways of dating earthquakes on the oblique-slip Hope fault, New Zealand: *Geological Society of America Abstracts with Programs*, v. 23, no 5, p. 168.
- Bull, W. B., 1991b, Geomorphic responses to climatic change: New York, Oxford University Press, 326 p.
- Bull, W. B., 1994, Avoiding pitfalls in lichenometry: *Geological Society of America Abstracts with Programs*, v. 26, no 7, p. 96.
- Bull, W. B., 1996a, Prehistorical earthquakes on the Alpine fault, New Zealand: *Journal of Geophysical Research, Solid Earth Special Section, Paleoseismology*, v. 101(B3), p. 6037–6050.
- Bull, W. B., 1996b, Dating San Andreas fault earthquakes with lichenometry: *Geology*, v. 24, p. 111–114.
- Bull, W. B., 1997, Lichenometry—A new way of dating and locating prehistorical earthquakes, in Sowers, J. M., Noller, J. S., and Lettis, W. R., eds., *Dating and earthquakes: Review of Quaternary geochronology and its application to paleoseismology*: U.S. Nuclear Regulatory Commission Report NUREG/CR 5562, p. 3–67–3–76.
- Bull, W. B., King, J., Kong, F., Moutoux, T., and Phillips, W. M., 1994, Lichen dating of coseismic landslide hazards in alpine mountains: *Geomorphology*, v. 10, p. 243–264.
- Bull, W. B., Schlyter, P., and Brogaard, S., 1995, Lichenometric analysis of the Kärkerieppe slush-avalanche fan, Kärkevage, Sweden: *Geografiska Annaler*, v. 77A, p. 231–240.
- Burrows, C. J., 1975, A 500 year old landslide in the Acheron River Valley, Canterbury: *New Zealand Journal of Geology and Geophysics*, v. 18, p. 357–360.
- Burrows, C. J., Duncan, K. W., and Spence, J. R., 1990, Aruanui vegetation history of the Arrowsmith Range, Canterbury. II. Revised chronology for moraines of the Cameron Glacier: *New Zealand Journal of Botany*, v. 28, p. 455–466.
- Conere, B. M., 1992, Population dynamics of a lowland rimu forest, South Westland, New Zealand [Master's thesis]: Christchurch, New Zealand, University of Canterbury, 102 p.
- Cowan, H. A., 1989, An evaluation of the late Quaternary displacements and seismic hazard associated with the Hope and Kakapo faults, Amuri District, North Canterbury [M.Sc. thesis]: Christchurch, New Zealand, University of Canterbury, 230 p.
- Cowan, H. A., 1991, The North Canterbury earthquake of September 1, 1888: *Journal of the Royal Society of New Zealand*: v. 21: p. 1–12.
- Cowan, H. A., 1994, Field Guide to New Zealand active tectonics: General Assembly of the International Association of Seismology and Physics of the Earth's Interior, 27th, Royal Society of New Zealand Miscellaneous Series 27.
- Cowan, H. A., and McGlone, M. S., 1991, Late Holocene displacements and characteristic earthquakes on the Hope River segment of the Hope fault, New Zealand: *Journal of the Royal Society of New Zealand*, v. 21, p. 373–384.
- Curry, R. R., 1969, Holocene climatic and glacial history of the central Sierra Nevada, California, in Schumm, S. A., and Bradley, W. C., eds., *United States contributions to Quaternary research: Geological Society of America Special Paper 123*, p. 1–47.
- Denton, G. H., and Karlen, W., 1973, Lichenometry; its application to Holocene moraine studies in southern Alaska and Swedish Lapland: *Arctic and Alpine Research*, v. 5, p. 347–372.
- Dowdrick, D. J., and Smith, 1990, E. G. C., 1990, Surface wave magnitudes of some New Zealand earthquakes, 1901–1988: *Bulletin of the New Zealand National Society of Earthquake Engineering*, v. 23, p. 198–210.
- Downs, G. L., 1995, Atlas of isoseismal maps of New Zealand earthquakes: *New Zealand Institute of Geological and Nuclear Sciences Monograph 11*, 304 p.
- Draper, N. R., and Smith, H., 1966, *Applied Regression Analysis*. New York, John Wiley and Sons, 407 p.

- Eiby, G. A., 1968, An annotated list of New Zealand earthquakes, 1460–1965: *New Zealand Journal of Geology and Geophysics*, v. 11, p. 630–647.
- Hanks, T. C., and Kanamori, H., 1979, A moment magnitude scale: *Journal of Geophysical Research* v. 84, p. 2981–2987.
- Innes, J. L., 1983, Lichenometric dating of debris-flow activity in the Scottish highlands: *Earth Surface Processes and Landforms*, v. 8, p. 579–588.
- Innes, J. L., 1984, The optimal sample size in lichenometric studies: *Arctic and Alpine Research*, v. 16, p. 233–244.
- Innes, J. L., 1985a, Lichenometry: Progress in Physical Geography, v. 9, p. 187–254.
- Innes, J. L., 1985b, A standard *Rhizocarpon* nomenclature for lichenometry: *Boreas*, v. 14, p. 83–85.
- Innes, J. L., 1985c, An examination of some factors affecting the largest lichens on a substrate: *Arctic and Alpine Research* v. 17, p. 99–106.
- Innes, J. L., 1986, The use of percentage cover measurements in lichenometric dating: *Arctic and Alpine Research* v. 18, p. 209–216.
- Innes, J. L., 1988, The use of lichens in dating, in Galun, M., ed., *CRC handbook of lichenology*: Boca Raton, Florida, CRC Press, v. III, p. 75–91.
- Jochimsen, M., 1973, Does the size of lichen thalli really constitute a valid measure for dating glacial deposits?: *Arctic and Alpine Research* v. 5, p. 417–424.
- Keefer, D. K., 1984, Landslides caused by earthquakes: *Geological Society of America Bulletin*, v. 95, p. 406–421.
- Keefer, D. K., 1994, The importance of earthquake-induced landslides to long term slope erosion and slope-failure hazards in seismically active regions: *Geomorphology*, v. 10, p. 265–284.
- Koerner, R. M., 1980, The problem of lichen-free zones in Arctic Canada: *Arctic and Alpine Research* v. 12, p. 87–94.
- Locke, W. W., III, Andrews, J. T., and Webber, P. J., 1979, A manual for lichenometry: *British Geomorphological Research Group Technical Bulletin* 26, 47 p.
- Luckman, B. H. and Fiske, C. J., 1995, Estimating long-term rockfall accretion rates by lichenometry, in Slaymaker, H. O., ed., *Steepland geomorphology*: New York, J. Wiley and Sons, p. 233–255.
- Mahaney, W. C., 1987, Lichen trimlines and weathering features as indicators of mass balance changes and successive retreat stages of the Mer de Glace in the Western Alps: *Zeitschrift für Geomorphologie*, v. 31, p. 411–418.
- Mandel, John, 1964, *The statistical analysis of experimental data*: New York, Dover Publications, 410 p.
- Matthews, J. A. 1974, Families of lichenometric dating curves from the Storbreen gletschervorfeld, Jutulheimen, Norway: *Norsk Geografiska Tidsskrift*, v. 28, p. 215–235.
- Matthews, J. A., and McCarroll, D., 1994, Snow-avalanche impact landforms in breheimen, southern Norway: Origin, age and paleoclimatic implications: *Arctic and Alpine Research*, v. 26, p. 103–115.
- McCalpin, J. P., editor, 1996, *Paleoseismology*: New York, Academic Press, 588 p.
- McCarroll, D., 1993, Modelling late-Holocene snow-avalanche activity—Incorporating a new approach to lichenometry: *Earth Surface Processes and Landforms*, v. 18, p. 527–539.
- McCarroll, D., 1994, A new approach to lichenometry: Dating single-age and diachronous surfaces: *The Holocene*, v. 4 p. 383–396.
- McGlone, M. S., 1979, The Polynesian settlement of New Zealand in relation to environmental and biotic changes, in Rudge, M. R., ed., *Moas, mammals, and climate in the ecological history of New Zealand*: *New Zealand Journal of Ecology*, v. 12, p. 15–129.
- New Zealand Meteorological Service, 1985, 1951–80 climate maps: Miscellaneous Publication 175, parts 4 and 6, scale 1:2 000 000.
- Officers of the New Zealand Geological Survey, 1985, Late Quaternary tectonic map of New Zealand (second edition): *New Zealand Geological Survey Miscellaneous Publication* 175, parts 4 and 6.
- Orwin, J. 1970, Lichen succession on recently deposited rock surfaces: *New Zealand Journal of Botany*, v. 8, p. 452–477.
- Orwin, J., 1971, The effect of environment on assemblages of lichens growing on rock surfaces: *New Zealand Journal of Botany*, v. 10, p. 37–47.
- Poelt, J., 1988, *Rhizocarpon* Ram. em. Th. Fr. subgen. *Rhizocarpon*: *Arctic and Alpine Research*, v. 20, p. 292–298.
- Porter, S. C., 1981, Lichenometric studies in the Cascade Range of Washington: Establishment of *Rhizocarpon geographicum* growth curves at Mount Rainier: *Arctic and Alpine Research*, v. 13, p. 11–23.
- Porter, S. C., and Orombelli, G., 1981, Alpine rockfall hazards: *American Scientist*, v. 69, p. 67–75.
- Press, W. H., Teukolsky, S. A., Vetterling, W. T., and Flannery, B. P., 1992, *Numerical recipes in Fortran* (second edition): Cambridge, England, Cambridge University Press, 963 p.
- Proctor, M. C. F., 1983, Sizes and growth-rates of the lichen *Rhizocarpon geographicum* on the moraines of the glacier De Valsorey, Switzerland: *Lichenologist*, v. 15, p. 249–261.
- Rapp, A., 1960, Recent development of mountain slopes in Kärkevagge and surroundings, northern Scandinavia: *Geografiska Annaler*, v. 42, p. 71–200.
- Rapp, A., 1981, Alpine debris flows in north Scandinavia, morphology and dating by lichenometry: *Geografiska Annaler*, v. 63A, p. 183–196.
- Selby, S. M., 1970, *CRC standard mathematical tables*, student edition (18th edition): Cleveland, Ohio, Chemical Rubber Company, 724 p.
- Silverman, B. W., 1986, *Density estimation for statistics and data analysis*: London, Chapman and Hall, 175 p.
- Smiley, T. L., 1953, The geology and dating of Sunset Crater, Flagstaff, Arizona, in *New Mexico Geological Society Field Conference Guidebook*, 9th, Black Mesa Basin, p. 186–190.
- Smirnova, T. Y., and Nikonov, A. A., 1990, A revised lichenometric method and its application dating great past earthquakes: *Arctic and Alpine Research*, v. 22, p. 375–388.
- Spence, J. R., and Mahaney, W. C., 1988, Growth and ecology of *Rhizocarpon* section *Rhizocarpon* on Mount Kenya, East Africa: *Arctic and Alpine Research*, v. 20, p. 237–242.
- Speight, R., 1933, The Arthur's Pass earthquake of 9 March, 1929: *New Zealand Journal of Science and Technology*, v. 15, p. 173–182.
- Stuiver, M. and Reimer, P. J., 1993, Extended ^{14}C data base and revised CALIB 3.0 ^{14}C age calibration program: *Radio-carbon* v. 35, p. 215–230.
- Titterton, D. M., Smith, A. F. M., and Makov, U. E., 1985, *Statistical analysis of finite mixture distributions*: New York, John Wiley and Sons, 243 p.
- Van Dissen, R. J., and Yeats, R. S., 1991, Hope fault, Jordan thrust, and uplift of the Seaward Kaikoura Range: *Geology*, v. 19, p. 393–396.
- Werner, A. 1990, Lichen growth rates for the northwest coast of Spitsbergen, Svalbard: *Arctic and Alpine Research* v. 22, p. 129–140.
- Whitehouse, I. E., 1981, A large rock avalanche in the Craigieburn Range, Canterbury: *New Zealand Journal of Geology and Geophysics*, v. 24, p. 415–421.
- Whitehouse, I. E., 1983, Distribution of large rock avalanche deposits in the central Southern Alps, New Zealand: *New Zealand Journal of Geology and Geophysics*, v. 26, p. 271–279.
- Whitehouse, I. E., McSaveney, M. J., and Chinn, T. J., 1983, Diachronous talus surfaces in the Southern Alps, New Zealand: *Arctic and Alpine Research* v. 15, p. 53–64.
- Wieczorek, G. F., and Jäger, Stefan, 1996, Triggering mechanisms and depositional rates of postglacial slope-movement processes in the Yosemite Valley, California: *Geomorphology*, v. 15, p. 17–31.
- Wieczorek, G. F., Snyder, J. B., Alger, C. S. and Isaacson, K. A., 1992, Rock falls in Yosemite Valley: U.S. Geological Survey Open-File Report 92–387, 136 p.
- Williams, L. D., 1978, The Little Ice Age glaciation level on Baffin Island, arctic Canada: *Palaeogeography, Palaeoclimatology, Palaeoecology*, v. 25, p. 199–207.
- Winchester, V., 1984, A proposal for a new approach to lichenometry: *British Geomorphological Research Group Shorter Technical Methods*, v. 33, p. 3–20.
- Winchester, V., 1989, An evaluation of lichenometry, with field studies in Lappland, Britain, and the western Alps [Ph.D. thesis]: Oxford, United Kingdom, University of Oxford, v. I, p. 1–277, v. II, 1–175.
- Winchester, V., and Harrison, S., 1994, A development of the lichenometric method applied to dating of glacially influenced debris flows in southern Chile: *Earth Surface Processes and Landforms*, v. 19, p. 137–151.
- Yamaguchi, D. K., 1985, Tree-ring evidence for a two-year interval between recent prehistoric explosive eruptions of Mount St. Helens: *Geology*, v. 13, p. 554–557.

MANUSCRIPT RECEIVED BY THE SOCIETY SEPTEMBER 7, 1995

REVISED MANUSCRIPT RECEIVED MARCH 4, 1997

MANUSCRIPT ACCEPTED MAY 20, 1997